The *Caenorhabditis elegans* Ephrin EFN-4 Functions Non-cell Autonomously with Heparan Sulfate Proteoglycans to Promote Axon Outgrowth and Branching

Alicia A. Schwieterman,*[,1,2] Alyse N. Steves,*[,1,3] Vivian Yee,[†,1] Cory J. Donelson,*[,4] Melissa R. Bentley,* Elise M. Santorella,* Taylor V. Mehlenbacher,* Aaron Pital,* Austin M. Howard,* Melissa R. Wilson,* Danielle E. Ereddia,* Kelsie S. Effrein,[‡] Jonathan L. McMurry,* Brian D. Ackley,[‡] Andrew D. Chisholm,[§] and Martin L. Hudson*[,5]

*Department of Molecular and Cellular Biology, Kennesaw State University, Kennesaw, Georgia 30144, [†]Department of Molecular, Cell and Developmental Biology, University of California, Santa Cruz, California 95064, [‡]Department of Molecular Biosciences, University of Kansas, Lawrence, Kansas 66045, and [§]Division of Biological Sciences, University of California San Diego, La Jolla, California 92093

ORCID ID: 0000-0002-2628-035X (M.L.H.)

ABSTRACT The Eph receptors and their cognate ephrin ligands play key roles in many aspects of nervous system development. These interactions typically occur within an individual tissue type, serving either to guide axons to their terminal targets or to define boundaries between the rhombomeres of the hindbrain. We have identified a novel role for the *Caenorhabditis elegans* ephrin EFN-4 in promoting primary neurite outgrowth in AIY interneurons and D-class motor neurons. Rescue experiments reveal that EFN-4 functions non-cell autonomously in the epidermis to promote primary neurite outgrowth. We also find that EFN-4 plays a role in promoting ectopic axon branching in a *C. elegans* model of X-linked Kallmann syndrome. In this context, EFN-4 functions non-cell autonomously in the body-wall muscle and in parallel with HS modification genes and HSPG core proteins. This is the first report of an epidermal ephrin providing a developmental cue to the nervous system.

KEYWORDS ephrin; Eph receptor; heparan sulfate proteoglycan; axon outgrowth; axon branching

ACCURATE development of the central nervous system requires contributions both from the extracellular environment in the form of guidepost cues and secreted guidance molecules and from contact with adjacent neurons or other tissues in the form of cell-surface receptors that can detect and transduce navigation cues. Guideposts typically take the form of specific tissue types such as the ventral midline of *Caenorhabditis elegans* or *Drosophila*, which provides a permissive environment for neurons to migrate along, while secreted guidance molecules provide spatial information and navigation instructions in the form of repulsive or attractive cues (Chilton 2006; Killeen and Sybingco 2008). Many studies have identified how individual neurons and guidance cues act to provide spatial and navigation information, but how does a single cell that possesses multiple axon guidance receptors find its target when exposed to multiple guidance cues? The nervous system of the nematode *C. elegans* provides a simple and defined model to examine the interplay between multiple neuronal guidance systems. The morphology and connectivity of *C. elegans* neurons have been established by serial-section electron microscopy, and

doi: 10.1534/genetics.115.185298
Manuscript received November 24, 2015; accepted for publication December 2, 2015; published Early Online December 7, 2015.
Supporting information is available online at www.genetics.org/lookup/suppl/doi:10.1534/genetics.115.185298/-/DC1.
This work is dedicated to the fond memory of Vivian Yee, who passed away on November 23, 2010.
[1]These authors contributed equally to this work.
[2]Present address: Interdisciplinary Program in Biomedical Sciences, College of Medicine, University of Florida, Gainsville, FL 32610.
[3]Present address: Genetics and Molecular Biology Graduate Program, Emory University, Atlanta, GA 30322.
[4]Present address: Department of Biological Sciences, University of South Carolina, Columbia, SC 29208.
[5]Corresponding author: Department of Molecular and Cellular Biology, Kennesaw State University, Bldg. 12, Room SC507, 370 Paulding Ave., Kennesaw, GA 30144. E-mail: mhudso28@kennesaw.edu

the *C. elegans* genome possesses orthologs of most vertebrate axon guidance and guidepost genes (White *et al.* 1986; Bargmann 1998; Chisholm and Jin 2005; Ackley 2014).

One of the most important classes of axon guidance molecules is the Eph receptor tyrosine kinases and their cognate ligands, the ephrins (Flanagan 2006; Lisabeth *et al.* 2013; Cayuso *et al.* 2015). Eph receptors and ephrins are required for the accurate connectivity of many parts of the vertebrate brain and also have roles in cell adhesion and embryonic morphogenesis (George *et al.* 1998; Chin-Sang *et al.* 1999; Chin-Sang *et al.* 2002; Klein 2012). We previously showed that the *C. elegans* ephrin EFN-4 functions in concert with the KAL-1/anosmin–heparan sulfate proteoglycan (HSPG) pathway to regulate neuroblast migration during embryonic development (Hudson *et al.* 2006). Anosmin is an extracellular matrix molecule that is highly conserved between humans and *C. elegans* (Bülow *et al.* 2002; Rugarli *et al.* 2002; Hu *et al.* 2003). Mutations in the human KAL1/anosmin gene lead to X-linked Kallmann syndrome, which is characterized by loss of sense of smell and the failure to undergo spontaneous puberty (Kallmann *et al.* 1944; Franco *et al.* 1991; Legouis *et al.* 1991; Dodé and Hardelin 2009). Curiously, rodents appear to lack orthologs of KAL1, making *C. elegans* one of the few model systems with which to investigate this disease. Overexpression of KAL-1 in the *C. elegans* central nervous system creates a highly penetrant, cell-autonomous ectopic branching phenotype (Bülow *et al.* 2002). This phenotype is strongly suppressed by mutations in HS modification enzymes, and in vitro binding studies have confirmed that KAL-1 can bind the HSPGs *sdn-1*/syndecan and *gpn-1*/glypican (Bülow *et al.* 2002; Hudson *et al.* 2006; Tornberg *et al.* 2011). HSPGs are required for many aspects of nervous system development in both vertebrates and invertebrates, including cell migration, axon guidance, and synaptogenesis (Rhiner *et al.* 2005; Van Vactor *et al.* 2006; Gysi *et al.* 2013; Kinnunen 2014; Blanchette *et al.* 2015). Considering the importance of both HSPGs and Eph/ephrin signaling during nervous system development, surprisingly little research has been dedicated to possible interactions between these pathways (Irie *et al.* 2008; Holen *et al.* 2011). In this study, we focus on the interplay between ephrins and HSPGs in the development of *C. elegans* AIY interneurons. We show that the ephrin EFN-4 is required non-cell autonomously to promote AIY primary neurite outgrowth, functioning in parallel with SDN-1/syndecan in this process. We also show that, in a *C. elegans* model of X-linked KS, EFN-4 plays a role in promoting AIY ectopic neurite branching, where it again functions non-cell autonomously. Finally, we show that SDN-1/syndecan and GPN-1/glypican have cell-autonomous yet mutually antagonistic roles in ectopic neurite formation. This is the first report of an ephrin acting non-cell autonomously from the epidermis to regulate neurite outgrowth and branching.

Materials and Methods

Strains and maintenance

C. elegans strains were grown on nematode growth medium plates (NGM Lite) at 20° according to Brenner (1974). All analyses were conducted at 20° unless otherwise noted. The following mutations were used in the course of this work: LGI—*kal-1(gb503)*; *mab-20(ev574)*; LGII—*vab-1(e2027)*; *unc-52(e998)*; LGIII—*hse-5(tm472)*; LGIV—*efn-4(bx80*, *e36*, *e660*, *e1746ts*, *ju134)*, *lad-2(tm3056)*, *sax-7(nj13)*; LGX—*sul-1(gk151)*, *hst-2(ok595)*, *hst-6(ok273)*, *sdn-1(ok449*, *zh20)*, *gpn-1(ok377)*, and *lon-2(e678)*. The following transgenes were used in the course of this work: LGII—*juIs76[P-unc-25-GFP + lin-15(+)]*; LGIV—*mgIs18[P-ttx-3-GFP]*, *otIs76[P-ttx-3-kal-1 (+) + P-unc-122-GFP]*, *juIs109[P-efn-4-efn-4*::*GFP + lin-15(+)]*, *oxTi420[P-eft-3-mCherry*::*tbb-2*-3′UTR + *Cbr-unc-119(+)]*; LGX—*oxIs12[P-unc-47-GFP lin-15(+)]*, *otEx331[P-lad-2-GFP + pha-1(+)]*.

The following extrachromosomal arrays were generated in the course of this work: *kenEx4*, *kenEx5*, *kenEx6 [P-myo-3-efn-4 + P-myo-3-mCherry]*; *kenEx9*, *kenEx10*, *kenEx11 [p-myo-2-efn-4 + P-myo-2*::*mCherry]*; *kenEx12*, *kenEx13*, *kenEx14 [efn-4 genomic + P-ttx-3-RFP]*; *kenEx16*, *kenEx17*, *kenEx18 [P-ttx-3-lon-2 + P-ttx-3-RFP]*; *kenEx19*, *kenEx20 [P-unc-119-efn-4 + P-ttx-3*::*RFP]*; *kenEx21*, *kenEx23*, *kenEx30 [P-elt-3-efn-4 + sur-5*::*GFP + P-ttx-3-RFP]*; *kenEx27*, *kenEx28*, *kenEx29 [P-elt-3-lon-2 cDNA + P-ttx-3-RFP]*; *juEx1335*, *juEx1336*, *juEx1337 [P-ttx-3-GFP*::*sdn-1 cDNA + P-ttx-3-RFP]*; *juEx1338*, *juEx1339*, *juEx1340 [P-gpn-1-GFP*::*gpn-1 cDNA + P-ttx-3-RFP]*; *juEx1341*, *juEx1342*, *juEx1343[P-AIY-efn-4 cDNA + P-ttx-3-RFP]*; *juEx1358*, *juEx1359*, *juEx1360 [P-ttx-3-gpn-1 cDNA + P-ttx-3-RFP]*; *lhEx174*, *lhEx175*, and *lhEx176 [P-lon-2-lon-2 cDNA + P-ttx-3-RFP]*.

Neuroanatomy

Neuronal morphology was scored using GFP or RFP expression from reporter genes. Animals were imaged either directly using a Zeiss Axioskop compound microscope or off-line from z-stacks of images acquired on a Zeiss LSM700 confocal microscope. Only axon branches exceeding 5 μm in length were included for analysis (Bülow *et al.* 2002). Distance was measured with Zeiss ZEN Blue software tools or the Segmented Line function of ImageJ (Rasband 1997–2014). Primary neurite outgrowth defects were scored as "shortstop" if they failed to reach their terminal target on the dorsal side of the nerve ring as defined by a visible gap of >3 μm.

Transgenic rescue of efn-4 and HSPG phenotypes

To assay for rescue of AIY phenotypes, transgenic lines were generated bearing either genomic clones or tissue-specific rescue plasmids in conjunction with a co-injection marker. All plasmids were generated in this work unless otherwise noted: pCZ148 (*efn-4* genomic clone; Chin-Sang *et al.* 2002), pMH340-3 (*P-ttx-3-efn-4* cDNA), pMH838 (*P-unc-119-efn-4* cDNA), pMH853 (*P-myo-2-efn-4* cDNA), pLC681 (*P-myo-3-efn-4* genomic, kind gift of Lihsia Chen), pMH833 (*P-elt-3-efn-4* cDNA), pMH306-7 (*P-ttx-3-GFP*::*sdn-1* cDNA), pMH265 (*P-gpn-1-GFP*::*gpn-1 cDNA*), pMH274 (*P-ttx-3-gpn-1* cDNA), pHW474 (*P-lon-2-lon-2* cDNA, Gumienny *et al.* 2007), pTG102 (*P-elt-3-lon-2* cDNA; Gumienny *et al.* 2007), and pMH644 (*P-ttx-3-lon-2* cDNA). *efn-4* plasmids were injected at

0.5, 1, or 5 ng·μl^{-1} into *efn-4(bx80) mgIs18 otIs76*. HSPG plasmids were injected into *hspg(null) mgIs18 otIs76* at 1 or 5 ng·μl^{-1}.The following co-injection plasmids were used: pTTX-3-RFP (AIY neuron RFP; Hobert *et al.* 1997), pTG96 (all nuclei GFP; Yochem *et al.* 1998), pPD131-68 (body-wall muscle mCherry, kind gift of A. Fire), pPD95-91 (pan-neuronal GFP; Fire *et al.* 1990), and pBA183 (pharyngeal mCherry). Plasmid construction details and sequences are available on request. See Supporting Information, Table S1 and Table S2, for details of *efn-4* and HSPG transgenic line construction.

Statistical analysis

Statistical significance was determined using the Z-test with an α-level of 0.05. Differences were considered significant if $P < 0.05$ (*), $P < 0.01$ (**), or $P < 0.001$ (***). Error bars on graphs show the standard error of proportion. Bonferroni corrections for multiple comparisons were applied where appropriate.

Expression plasmid construction

The following plasmids were used to express and secrete proteins from 293T cells: pCZ144 (VAB-1 extracellular domain::AP; Chin-Sang *et al.* 1999), pMH180 (Fc::mycHis), pMH873 (EFN-1::Fc::mycHis), and pMH874 (EFN-4::Fc::mycHis). Note that EFN-1 is also known as VAB-2. See File S1 for details on plasmid construction. Plasmid sequences are available on request.

Cell culture

HEK293T cells were maintained in Dulbecco's Modified Eagle's Medium (Caisson Laboratories Inc.) supplemented with 10% ultralow IgG Fetal Bovine Serum (Life Technologies), 1 mM L-glutamine (Caisson Laboratories Inc.), and 1× penicillin–streptomycin (Caisson Laboratories Inc.).

Transient transfection of EFN-1, EFN-4, and VAB-1 expression plasmids

Expression plasmids were transfected into HEK293T cells using Lipofectamine 2000 Transfection Reagent (Life Technologies) and Opti-MEM Reduced Serum Medium (Life Technologies) according to the manufacturer's protocol. Final DNA concentrations were 10 ng·μl^{-1}. Transfections were incubated at 37° in 5% CO_2 atmosphere for 48 hr. Supernatants were harvested, centrifuged to remove cellular debris, and then either used directly or concentrated using a 10-kDa cut-off centrifugal filter (Centricon). Protein production was confirmed by either Western blotting to detect myc-tags of the transfected ephrin-Fc proteins or by an AP-turnover assay for VAB-1(ECD)::AP.

Biolayer interferometry

Biolayer interferometry measurements were made on a FortéBio Octet-QK instrument using anti-human IgG Fc capture (AHC) biosensors (FortéBio, Inc.). Assays were performed in 96-well microplates at 25°. All volumes were 200 μl. Biosensors were conditioned for 3 min in Opti-MEM media prior to loading. Ephrin-Fc ligands or Fc controls were bound onto AHC biosensors for 60 min and then a baseline was established in Opti-MEM for 15 min. Sensors were then incubated in VAB-1::AP tissue culture supernatant for 60 min (analyte association phase), followed by incubation in Opti-MEM for 60 min (dissociation phase).

Results

Our previous work showed that *efn-4* mutations synergize with *kal-1* in neuroblast migrations during embryonic morphogenesis, suggesting that EFN-4 and KAL-1 play closely related roles in cell migration or adhesion (Hudson *et al.* 2006). To learn whether EFN-4 and KAL-1 also function together in neural development, we tested whether *efn-4* mutations displayed genetic interactions with *kal-1(lf)* and *kal-1(gf)* mutations during axon outgrowth and branching. Table 1 summarizes the *efn-4* alleles used in this study.

EFN-4 is required for neural development

The AIY neurons are a bilaterally symmetric pair of interneurons that are born ~365 min post-fertilization (Bao *et al.* 2006; Murray *et al.* 2008). We used *mgIs18*, an AIY-specific GFP-transgene driven from a *ttx-3*-intronic enhancer element, to monitor development of the AIY interneurons in embryos, larvae, and adults (Altun-Gultekin *et al.* 2001). Following ventral enclosure, the AIY cell bodies lie adjacent to myoblasts, the developing pharynx, and also the ventral epidermis. They begin to extend their primary neurites anteriorly during the lima bean stage of embryonic development and then dorsally at the 1.5-fold stage (Christensen *et al.* 2011 and M. L. Hudson, unpublished observations). The AIYL and R cell bodies ultimately lie in the ventral ganglion beneath the posterior pharyngeal bulb. Their main axons, which we refer to in this study as the primary neurites, converge anteriorly at a plexus-like area where they enter the nerve ring. Within the plexus the AIYs are flattened immediately adjacent to the cephalic sheath cells, where they occasionally extend very short collateral branches. After entering the nerve ring the AIY primary neurites extend circumferentially to the dorsal midline where they contact one another via a gap junction (Figure 1, A and B; White *et al.* 1986).

We find that all *efn-4* loss-of-function alleles show strong premature axon termination defects in the AIY interneurons, which manifest as failure of the primary neurites to meet at the dorsal midline (Figure 1, D and F). We refer to this as a shortstop phenotype, as the overall trajectory of the axons is correct, but the axons stop short of their correct termination site. The phenotypic penetrance roughly correlates with the allelic strength described by Chin-Sang *et al.* (2002) with *bx80* and *e660* showing 34 and 53% shortstop phenotype respectively, whereas the *e1746ts* allele shows only 21% shortstop. This is in contrast to *mgIs18* controls that show no shortstop phenotype (90 animals scored). We also observed that AIY primary neurite outgrowth defects in *efn-4* mutants were intrinsically temperature sensitive, irrespective

Table 1 Summary of *efn-4* alleles used in this study

efn-4 allele	Nature of mutation	Phenotype[a]
e1746	A75V	Weak (temperature sensitive)
e660	P54L	Intermediate
bx80	1839-bp deletion	Strong (predicted null)
e36	Y69ochre	Strong
ju134	T72I	Strong

The *bx80* deletion removes all of exon 2 from the *efn-4* locus and is predicted to create a frameshift at the exon 1-to-exon 3 splice junction, generating a premature stop codon.

[a] Phenotypic penetrance based on embryonic lethality data summarized in Chin-Sang *et al.* (2002).

of the allele tested (Table S3). For example, *efn-4(bx80)* showed only 23% outgrowth defects at 15° but increased to 34 and 32% at 20° and 25°, respectively. For consistency, all remaining data were scored at 20°.

We also assayed *efn-4* shortstop phenotypes in a *kal-1(gf)* background (Figure 1, E and F). Again, all three *efn-4* alleles showed highly penetrant shortstop phenotypes, although *efn-4(e1746ts)* mutants displayed significantly stronger phenotypes in a *kal-1(gf)* background, whereas *efn-4(e660)* were significantly weaker. These differences may reflect the overall sensitivity of this phenotype to temperature variation. Considering that all three *efn-4* alleles examined had strong shortstop phenotypes irrespective of the *kal-1(gf)* background, and that *kal-1(gf)* alone has no phenotype, we conclude that KAL-1 overexpression has no overt influence on primary neurite outgrowth. For convenience, all remaining experiments on *efn-4* function were carried out in the *kal-1(gf)* background.

To confirm that EFN-4 is required for AIY primary neurite outgrowth, we used germ-line microinjection to reintroduce an *efn-4* genomic clone into *kal-1(gf) efn-4(bx80)* null mutants. This rescued the AIY shortstop phenotype from 50% (27/54 animals tested) down to around 17% depending on the transgenic line in question (Figure 1F, three independent lines, $P < 0.01$). These rescues support our genetic loss-of-function analysis, further confirming that EFN-4 is required for AIY primary neurite outgrowth.

EFN-4 promotes D-class motorneuron outgrowth but not axon guidance

EFN-4 is expressed in multiple tissues at various stages of the *C. elegans* life cycle and, as such, could be required for the development of many neuron types including the ventral nerve cord (Chin-Sang *et al.* 2002). We used the *P-unc-25-GFP* reporter, *juIs76*, to investigate whether EFN-4 has roles in shaping the morphology of D-type motorneurons (Zhen and Jin 1999). The six dorsal D-type (DD) neurons migrate to the ventral midline during midembryogenesis and extend an axon anteriorly, which then branches midway along the axon, and extends a commissural process circumferentially around the worm until it meets the dorsal midline where it again branches, extending processes to both the anterior and posterior (Figure 2A). DD neuron commissural migration is stereotyped in that the DD1 neuron extends its process to the left side of the animal, whereas DD2-6 extends commissures to the right side. The 13 ventral D-type (VD) neurons are born late in the L1 larval stage and share similar morphology and guidance choices to the DD neurons; VD1 extends a process to the left whereas VD2-13 extends processes to the right (White *et al.* 1976). In both DD and VD neurons, the anterior and posterior processes of each cell make a gap-junction contact with their respective anterior and posterior DD/VD neighbors and provide GABAergic inhibitory innervation to the body-wall muscles to promote smooth sinusoidal locomotion (White *et al.* 1976). In wild-type animals, the ventral and dorsal nerve cords appear as contiguous structures, with only 4% of animals (2/44) showing gaps in the dorsal D-neuron cord (Figure 2B). In *efn-4(bx80)*, 29% of animals (15/53) show at least one gap in dorsal cord morphology (Figure 2, C and D). In addition, 8% of animals (4/53) show a "crooked" dorsal cord phenotype (Figure 2C) as opposed to the linear dorsal cord seen in wild-type animals. We also examined left/right outgrowth choice of the commissural processes. In wild type, 7% of worms (3/47) show at least one axon where the commissural process navigates dorsally via the wrong side of the animal. In *efn-4* mutants, 9% of worms (5/58) show a commissural guidance defect (not significant). Taken together, we conclude that EFN-4 is required, in part, to promote the final stage of D-neuron outgrowth along the dorsal nerve cord, similar to its role in promoting the final stage of AIY primary neurite outgrowth, but that it has no role in axon guidance. While it is possible that EFN-4 is required for the development of other neural cell types beyond the AIY interneurons and D-motorneurons, the remainder of this work will focus solely on EFN-4's role in shaping AIY interneuron morphology.

EFN-4 is required to promote kal-1(gf) ectopic branching

We previously showed that *efn-4* mutants exhibit strong genetic interactions with *kal-1*/anosmin mutants during embryonic ventral neuroblast migrations (Hudson *et al.* 2006). Overexpression of KAL-1 in the AIY neurons causes highly penetrant cell-autonomous ectopic neurite branching (Bülow *et al.* 2002). The ectopic branches extend posteriorly from the ventral plexus of the AIYs and may represent hypertrophied versions of the small branches normally formed in this region. We confirmed that *P-AIY-kal-1* (*otIs76*) causes ectopic AIY branch formation and also observed ectopic branches emanating from AIY cell bodies and occasionally the nerve ring process (Figure 1C and Figure 3). We also found that ectopic branch formation is temperature sensitive (Table S4 lists all strains and AIY phenotypes scored at different temperatures during the course of this work). At 20° 55% of *mgIs18 otIs76* AIY neurons (84% of animals; $n = 153$) exhibited ectopic branches. We found that loss of function in *kal-1* partially suppresses this *kal-1(gf)* effect, supporting the interpretation that ectopic branches are due to excess of normal KAL-1 function. Interestingly, the *kal-1(lf)* mutation itself caused low-penetrance branching of AIYs, suggesting that either reduction or elevation of KAL-1 function may affect branching.

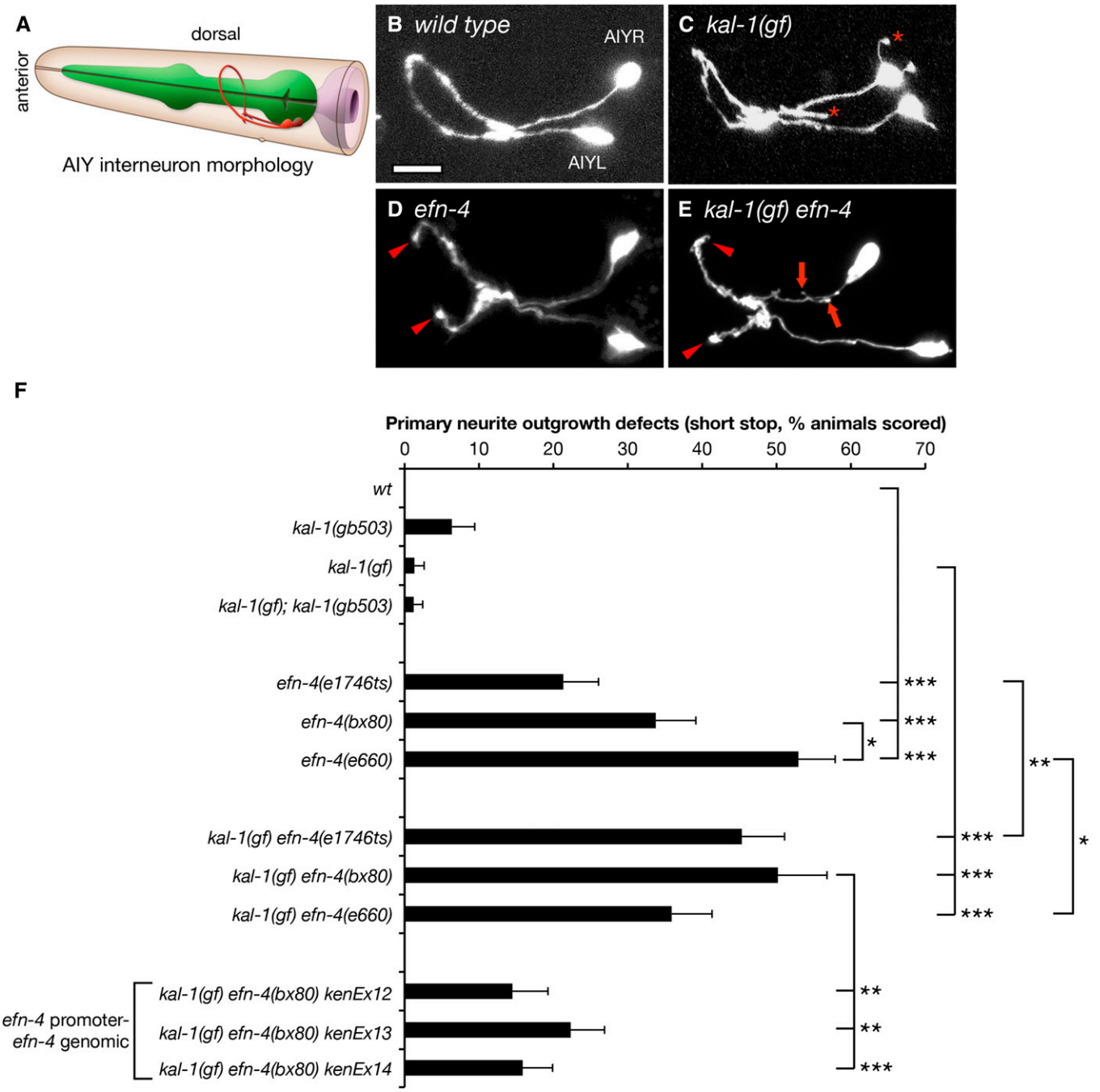

Figure 1 *efn-4* mutants have defects in AIY primary neurite outgrowth and suppress KAL-1-dependent axon branching. (A) Cartoon depiction of AIY interneuron morphology in relation to the pharynx and epidermis. AIY neurons are bilaterally symmetrical unipolar cells that extend a single axon anteriorly. The axons contact their contralateral partner on the ventral side of the nerve ring beneath the pharynx before extending anteriorly, where they again make contact on the dorsal side of the worm (image adapted from http://www.wormatlas.org). (B) Confocal micrograph of AIY neuron morphology in a wild-type background. (C) *kal-1(gf)* worms overexpress KAL-1 in the AIY neurons, causing a highly penetrant ectopic axon-branching phenotype (asterisks). (D) AIY neuron morphology in an *efn-4(bx80)* mutant background. Arrowheads show premature axon outgrowth termination, resulting in a failure to make contact on the dorsal side of the nerve ring. (E) *kal-1(gf)* axon branching is suppressed in *efn-4* mutants. Arrows show short, stubby axon branches. Arrowheads show premature axon termini. Bar, 10 μm. (F) Graph of AIY axon outgrowth defects in *efn-4* mutant backgrounds. All alleles tested show axon outgrowth defects and are generally more penetrant in a *kal-1(gf)* background. *kenEx12–14* are transgenic rescue arrays containing an *efn-4* genomic clone that includes 5 kb of the *efn-4* promoter region. Statistical significance was determined using the Z-test. *$P < 0.05$; **$P < 0.01$; ***$P < 0.001$. Error bars are standard error of proportion.

We next examined AIY ectopic branching in *kal-1(gf) efn-4(−)* lines. We found that four of five *efn-4* alleles significantly suppressed *kal-1(gf)* branching (Figure 1, C and E, and Figure 3). Reintroduction of an *efn-4* genomic clone into *kal-1(gf) efn-4(bx80)* mutants significantly rescues this phenotype ($P < 0.05$ for 3/3 lines tested; $n = 100$, 195, and 192

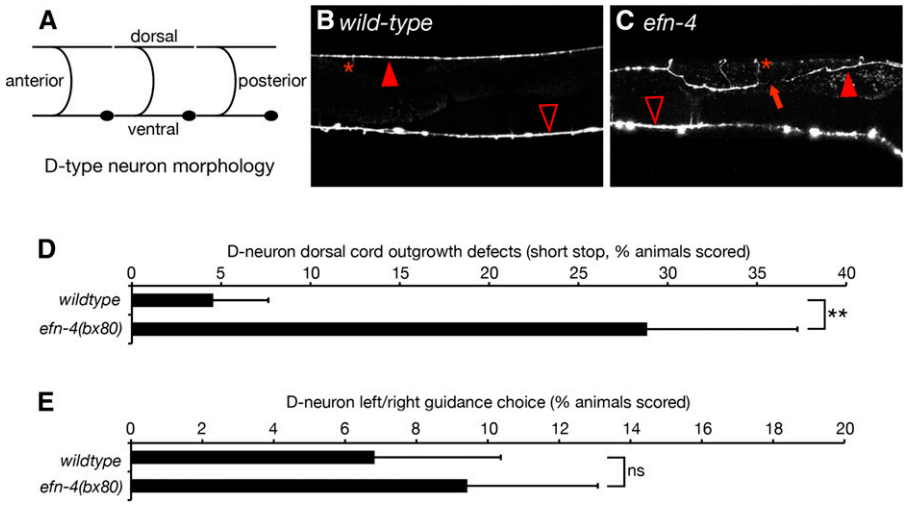

Figure 2 *efn-4* mutations show defects in D-neuron axon outgrowth. (A) Diagram of DD-neuron morphology (VD neurons are similar in shape but their commissures are located farther away from the cell body). The DD1 and VD1 commissural processes navigate to the dorsal side via the left side of the body whereas the remaining processes navigate dorsally via the right side. (B) Confocal micrograph of GFP expression from the D-neuron-specific GFP marker *juIs76[P-unc25-GFP]*. (C) *efn-4* mutants display defects in D-neuron outgrowth (arrow) and can also show twisted dorsal axon tracts. Solid arrowhead, dorsal nerve cord; open arrowhead, ventral nerve cord; asterisk, commissural processes. (D) Graph of D-neuron dorsal outgrowth defects. (E) Left/right commissural guidance decisions in wild-type versus *efn-4 (bx80)* mutants. Statistical significance was determined using the Z-test. $^{**}P < 0.01$. Error bars are standard error of proportion.

for *kenEx12–kenEx14*, respectively; Figure 3). From this, we conclude that EFN-4 contributes to *kal-1(gf)*-induced ectopic branching, but that other genes are likely to be required in this process.

To better understand which additional genes might contribute to AIY primary neurite extension and *kal-1(gf)*-induced ectopic branching, we examined AIY morphology in other genetic mutants known to affect axon outgrowth (Table 2). Both *plx-2*/plexin and *mab-20*/semaphorin have been implicated in EFN-4 function during neuroblast migration, male tail sensory ray formation, and axon guidance (Nakao *et al.* 2007; Wang *et al.* 2008). We found that *plx-2* mutants showed no defects in primary neurite outgrowth, nor did they affect *kal-1(gf)* ectopic axon branching. This was in sharp contrast to *mab-20* mutants, which showed highly penetrant primary neurite outgrowth defects, similar to *efn-4* mutants. This concurs with previous genetic studies, placing *efn-4* and *mab-20* in a common neurodevelopmental pathway (Chin-Sang *et al.* 2002; Ikegami *et al.* 2004; Nakao *et al.* 2007). The LAR-like receptor protein tyrosine phosphatase PTP-3 is required for embryonic morphogenesis, axon outgrowth, and synapse formation (Harrington *et al.* 2002; Ackley *et al.* 2005). We found that *ptp-3(mu256)* mutants also exhibit defects in both primary neurite outgrowth and *kal-1(gf)* ectopic branching. We did not attempt further analysis of *efn-4* and *ptp-3* genetic interactions due to the strong synthetic-lethal phenotype observed between *ptp-3(mu256)* and all *efn-4* alleles tested (R. Harrington and A. D. Chisholm, unpublished observations). Mutations in *unc-71* (a Disintegrin and Metalloprotease protein) and *cam-1*/Ror kinase also exhibited defects in either primary neurite outgrowth or suppressed *kal-1(gf)* ectopic branching. This is consistent with previous studies implicating both of these genes in shaping neuronal morphology (Huang *et al.* 2003; Kim and Forrester 2003; Hayashi *et al.* 2009; Kennerdell *et al.* 2009). A mutation in *sax-7*, the canonical L1-like cell adhesion molecule ortholog, showed no significant defects in primary neurite outgrowth although there was a significant increase in *kal-1(gf)* ectopic branching. However, we did observe low-penetrance cell-body positioning defects similar to those reported by others (Sasakura *et al.* 2005; Díaz-Balzac *et al.* 2015). Overall, these data indicate that multiple genes are required for both primary neurite outgrowth and *kal-1(gf)* ectopic axon branching in AIY neurons, in addition to EFN-4.

EFN-4 acts non-cell autonomously to promote AIY outgrowth and kal-1(gf) ectopic branching

As a GPI-linked cell-surface ephrin, EFN-4 might act cell autonomously or non-autonomously from an adjacent cell to promote axon outgrowth. To address this, we used tissue-specific promoters driving expression of an *efn-4* complementary DNA (cDNA) to determine which tissue EFN-4 is required in for AIY primary neurite outgrowth versus *kal-1(gf)*-dependent axon branching (Figure 4). Despite EFN-4's extensive expression in the nervous system (Chin-Sang *et al.* 2002), both AIY-specific and pan-neural *efn-4* expression failed to rescue primary neurite outgrowth defects, indicating that EFN-4 may be functioning non-cell autonomously (Figure 4A).

The close juxtaposition of AIY cell bodies to pharyngeal, body-wall muscle, and epidermal cells during neurite outgrowth suggested that one or more of these tissues could theoretically provide a non-cell autonomous cue for AIY neurite outgrowth. When we used the *myo-2* promoter to drive pharyngeal expression of an *efn-4* cDNA, no significant rescue of outgrowth defects was observed (0/3 lines, $n = 50$ animals per line). Expression of *efn-4* from a *myo-3* body-wall muscle-specific promoter also failed to show any rescue (0/3 lines tested, $n = 50$ animals per line). However, expression of *efn-4* from an *elt-3* epidermal-specific promoter showed significant rescue (3/3 lines tested, $n = 21$, 49, and 54 animals per line, respectively). Note that all three of the *P-elt-3-efn-4* lines showed high embryonic lethality and a fourth line (not shown) strongly selected against epidermal *efn-4* expression.

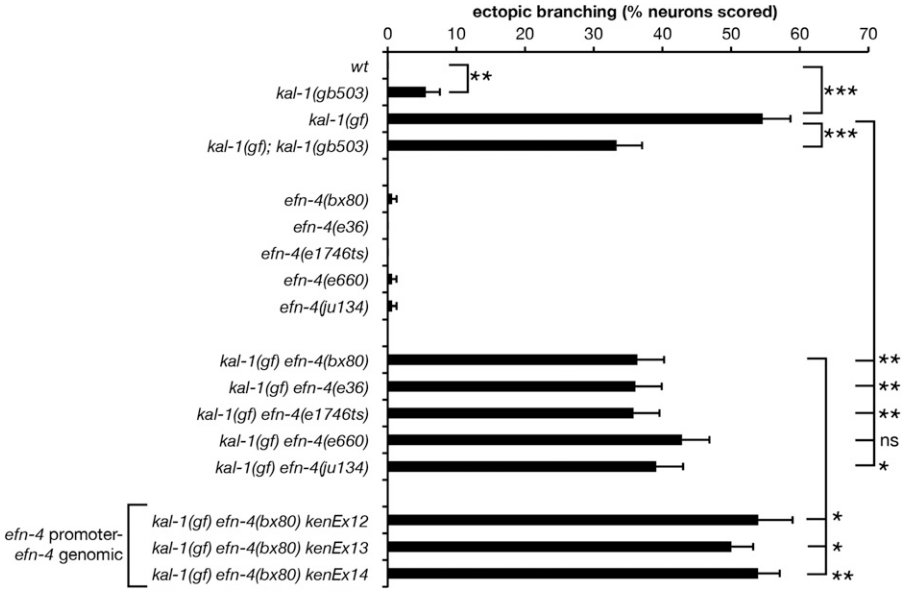

Figure 3 *efn-4* mutations suppress *kal-1(gf)*-induced axon branching. Four of five *efn-4* alleles tested significantly suppress *kal-1(gf)* ectopic axon branching relative to *kal-1(gf)* alone. *kenEx12–14* are transgenic rescue arrays containing an *efn-4* genomic clone that includes 5 kb of the *efn-4* promoter region. Statistical significance was determined using the Z-test. $*P < 0.05$; $**P < 0.01$; $***P < 0.001$. Error bars are standard error of proportion.

From this, we conclude that EFN-4 is required non-cell autonomously in the embryonic epidermis to promote AIY primary neurite outgrowth. We also conclude that embryonic development is highly sensitive to epidermal EFN-4 expression levels; the correct amount of EFN-4 in the appropriate tissue is sufficient to complete embryogenesis, but overexpression can cause a neomorphic embryonic lethal phenotype.

We also examined whether tissue-specific expression of *efn-4* could rescue *efn-4(bx80)* suppression of *kal-1(gf)*-dependent axon branching (Figure 4B). AIY-specific expression of *efn-4* led to increased but not significant suppression of branching in one of two lines tested, although pan-neural expression had no effect. Taken together, this suggests that EFN-4 is unlikely to be required in the nervous system for ectopic branch formation. Pharyngeal expression of *efn-4* showed a slight but not significant increase of branching in two of three lines tested. Intriguingly, expression of *efn-4* in the body-wall muscle rescued *kal-1(gf)* neurite branching in one of three lines tested with the other two lines approaching significance, but did not rescue body morphology defects seen in *efn-4* mutants (data not shown). This was in contrast to epidermal expression of *efn-4*, which did not significantly alter branching levels when compared to *efn-4(bx80)* alone. From this, we tentatively conclude that EFN-4 expression from body-wall muscle during early embryogenesis is required, in part, to promote *kal-1(gf)* axon branching. In addition, this suggests that *kal-1(gf)* ectopic branching is genetically separable from AIY primary neurite outgrowth.

Eph receptor VAB-1 plays a minor role in promoting AIY primary neurite outgrowth

If EFN-4 is required non-cell autonomously in the epidermis to promote AIY primary neurite outgrowth, then presumably it must function via one or more receptors on the AIY neurons. Previous work has identified multiple roles for the *C. elegans* Eph receptor VAB-1 during development, including embryonic morphogenesis, oocyte maturation, and amphid neuron axon guidance (George *et al.* 1998; Miller *et al.* 2003; Mohamed and Chin-Sang 2006; Ikegami *et al.* 2012; Grossman *et al.* 2013). VAB-1 can bind EFN-4 in vitro, making it an obvious candidate receptor (Wang *et al.* 1999). We confirmed this finding using biolayer interferometry, a form of optical biosensing similar to surface plasmon resonance (Abdiche *et al.* 2008; Wilson *et al.* 2010). EFN-1::Fc, EFN-4::Fc, or Fc control ligands were immobilized onto anti-human Fc capture probes and then exposed to tissue culture supernatants containing the VAB-1 extracellular domain fused to alkaline phosphatase (VAB-1::AP). We found similar association curves for VAB-1::AP binding to both EFN-1 and EFN-4 (Figure 5A) whereas Fc shows negligible association (the Fc-binding data were used to normalize for negative drift, and hence data are not shown). The dissociation curves for both EFN-1–VAB-1 and EFN-4–VAB-1 interactions were essentially flat, consistent with a very slow dissociation rate (Figure 5B). These data reconfirm that EFN-4 binds VAB-1 in vitro.

To ask whether VAB-1 plays any role in shaping AIY neuron development, we examined AIY morphology in a *kal-1(gf) vab-1(e2027)* null mutant background (George *et al.* 1998). In *kal-1(gf) vab-1(e2027)* animals, 15% of AIY neuron pairs (8/45) show short-stop defects during primary neurite outgrowth compared to 1% (1/76) of *kal-1(gf)* controls (Figure 5E). However, this phenotype is significantly less than that seen in *kal-1(gf) efn-4(bx80)* animals (50%, 27/54). This suggests that VAB-1 plays a minor part in promoting AIY primary neurite outgrowth and that it may function redundantly with one or more other receptors in this role. We were unable to assay whether *vab-1* and *efn-4* function together in a linear genetic pathway as *vab-1*; *efn-4* double-mutant combinations show strongly synergistic embryonic lethality, thus preventing genetic analysis of AIY morphology in adult animals (Chin-Sang *et al.* 2002).

Table 2 Other neurodevelopmental genes examined during the course of this work

Strain	Primary neurite outgrowth defects (%)	Total animals scored	Branched AIYs (%)	Total neurons scored
A. *kal-1(wt)*				
mgIs18	0.0	90	0	180
ptp-3(mu256)	13.3 (***)	75	1.3	150
plx-2(tm729)	0.0	75	0.0	150
spon-1(e2623)	0.0	76	1.3	152
mab-20 (ev574)	40.3 (***)	77	2.0	154
unc-71(ju156)	Not tested			
cam-1(gm122)	3.9	76	0.7	152
B. *kal-1(gf)*				
mgIs18 otIs76	1.3	75	54.6	152
ptp-3(mu256)	29.8 (***)	84	42.3 (*)	168
cle-1(ju34)	1.3	76	58.6	152
cle-1(cg120)	0.0	78	44.9	158
plx-2(tm729)	0.0	77	48.1	154
spon-1(e2623)	0.0	76	42.1 (*)	152
mab-20 (ev574)	Not tested			
unc-71(ju156)	29.9 (***)	77	42.2 (*)	154
cam-1(gm122)	3.9	77	39.6 (**)	154
sax-7(nj13)	5.4	74	73.0 (***)	148

(A) All *kal-1(wt)* strains have *mgIs18 [P-ttx-3-GFP]* in the background. (B) All *kal-1(gf)* strains contain *mgIs18 [P-ttx-3-GFP]otIs76[P-ttx-3-kal-1 P-unc-122-GFP]*. Statistical significance was determined using the Z-test. *$P < 0.05$; **$P < 0.01$; ***$P < 0.001$.

We also examined if VAB-1 plays a role in promoting the growth of *kal-1(gf)*-dependent ectopic neurites (Figure 5F). Fifty-five percent of *kal-1(gf) vab-1(e2027)* neurons examined (58/106) showed ectopic branching, which is the same as that seen in *kal-1(gf)*. This suggests that VAB-1 plays no part in ectopic neurite branching and is consistent with EFN-4 having VAB-1-independent roles. This result also suggests that there is an unidentified receptor for EFN-4 and provides further evidence that primary versus ectopic (secondary) neurite growth are genetically distinct processes.

Eph receptor VAB-1 is required for ventral plexus contact between AIY neurons

AIY neuron pairs have two contact points between the AIYL and AIYR cells; they initially touch each other in the ventral plexus and then grow apart, wrapping around the left and right sides of the pharynx, respectively, before contacting again on the dorsal side of the nerve ring via a gap junction (White *et al.* 1986). Although VAB-1 plays only a minor role in promoting primary neurite outgrowth, we find it plays a major role in organizing the plexus contact (Figure 5, D and G). Fifty percent of *kal-1(gf) vab-1(e2027)* animals (26/52) have a distinct gap between the AIY left and right cells at the plexus compared to 8% of *kal-1(gf)* controls (4/49) and 4% of *kal-1(gf) efn-4* mutants (2/54). The functional importance of an AIYL/R plexus contact in the normal physiology of these cells is not known.

We also found that AIY neuron cell bodies were frequently displaced anteriorly in *kal-1(gf) vab-1* mutants compared to wild type, whereas *kal-1(gf) efn-4* cell bodies were often displaced posteriorly (data not shown). Despite this, we did not see any correlations between the location of the cell body and whether there were defects in primary neurite outgrowth or AIYL/R plexus contact. In addition, *vab-1* mutants frequently display variably penetrant head morphology defects, which could in principle influence the shape of neurons in the head region (George *et al.* 1998; Tucker and Han 2008). However, we saw no correlation between head morphology defects and the presence of a ventral plexus gap between the AIYL and R neurons (5/9 animals with wild-type head morphology had plexus gaps compared to 20/47 animals that displayed a morphological defect).

L1CAM LAD-2 may inhibit AIY primary neurite outgrowth

efn-4 shows strong genetic interactions with the secreted semaphorin *mab-20* and has been shown to bind in a complex with the semaphorin receptor PLX-2 (Nakao *et al.* 2007). MAB-20 and PLX-2 also exhibit genetic and physical interactions with the L1CAM LAD-2 (Wang *et al.* 2008). Our data show that *mab-20* mutants exhibit strong AIY primary neurite shortstop defects, although PLX-2 has no obvious role in shaping AIY morphology (Table 2), raising the possibility that LAD-2 may be a receptor for EFN-4. We find that *lad-2(tm3056)* null mutants have no obvious defects in AIY primary neurite outgrowth when examined alone, but significantly suppress *efn-4* primary neurite defects in *efn-4*; *lad-2* double mutants (Figure 5E). Also, *vab-1*; *lad-2* double mutants are not significantly different from *vab-1* mutants alone. With regard to AIYL/R plexus contact, *lad-2* mutants are not significantly different from wild type and *vab-1*; *lad-2* double mutants display the same phenotype as *vab-1* mutants alone (27/54 *vab-1*; *lad-2* animals show a plexus gap phenotype compared to 26/52 *vab-1* mutants). These data suggest that LAD-2 may play a role in inhibiting AIY neuron primary outgrowth and that it functions antagonistically with EFN-4 in this process. We see no evidence of genetic interactions

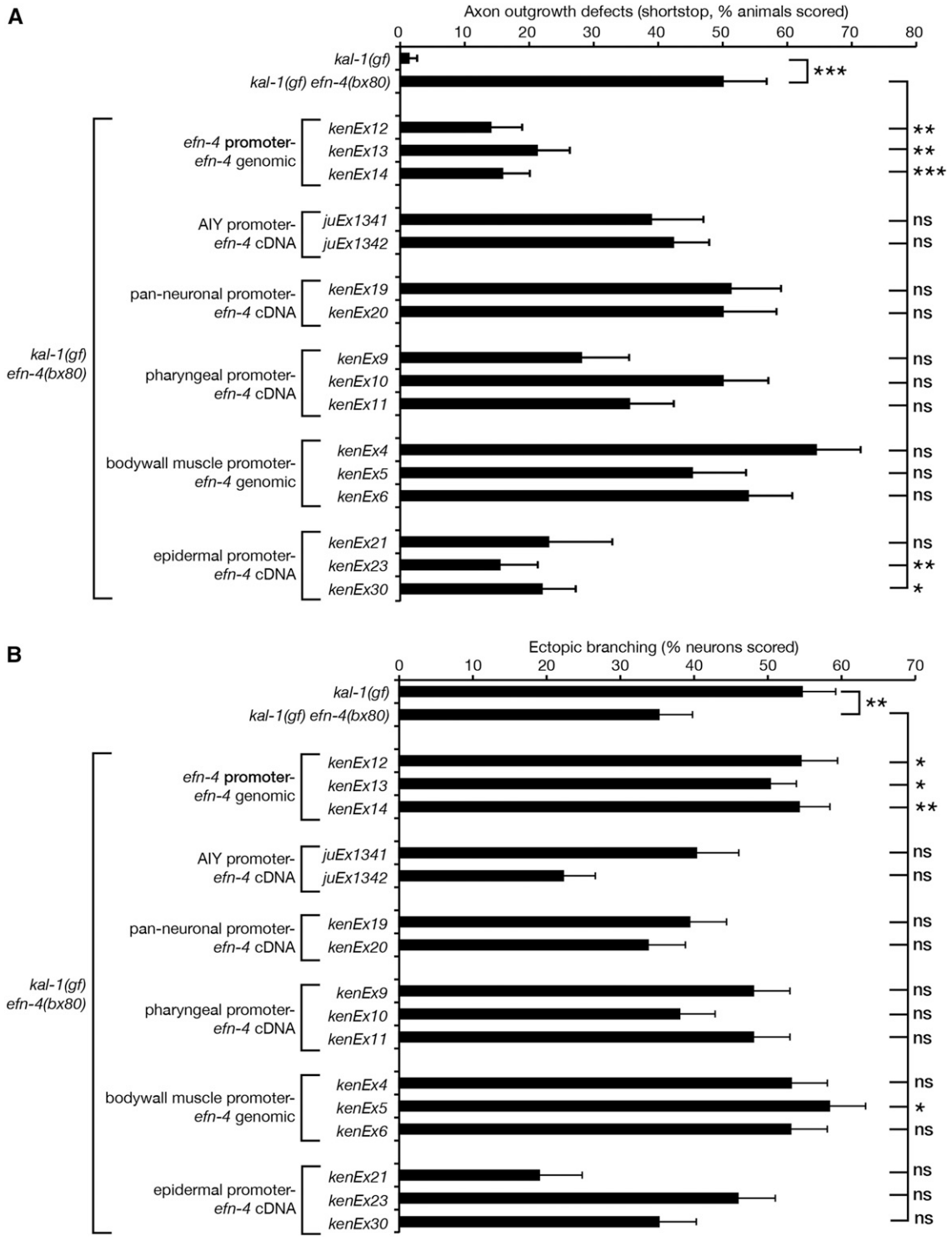

Figure 4 *efn-4* functions in the epidermis to promote AIY primary neurite outgrowth and in the body-wall muscle to promote *kal-1(gf)*-induced ectopic axon branching. Tissue-specific *efn-4* transgenic lines were generated to establish what tissue *efn-4* is required for (A) primary neurite outgrowth and (B) ectopic neurite branching. *efn-4* genomic rescue data from Figure 1 and Figure 3 are included for comparison. All strains contain *kal-1(gf)*, and all rescue lines are in a *kal-1(gf) efn-4(bx80)* background. A minimum of two transgenic lines was assayed for every construct. Statistical significance was determined using the Z-test. $*P < 0.05$; $**P < 0.01$; $***P < 0.001$. Error bars are standard error of proportion.

between *lad-2* and *kal-1(gf)* during ectopic neurite branching (Figure 5F). In addition, *lad-2* mutants have no obvious AIYL/R plexus contact defects (Figure 5G). As there is no evidence for LAD-2 expression in AIY neurons (Wang *et al.* 2008), we consider it unlikely that LAD-2 is a cell-autonomous receptor for EFN-4 during AIY neuronal development.

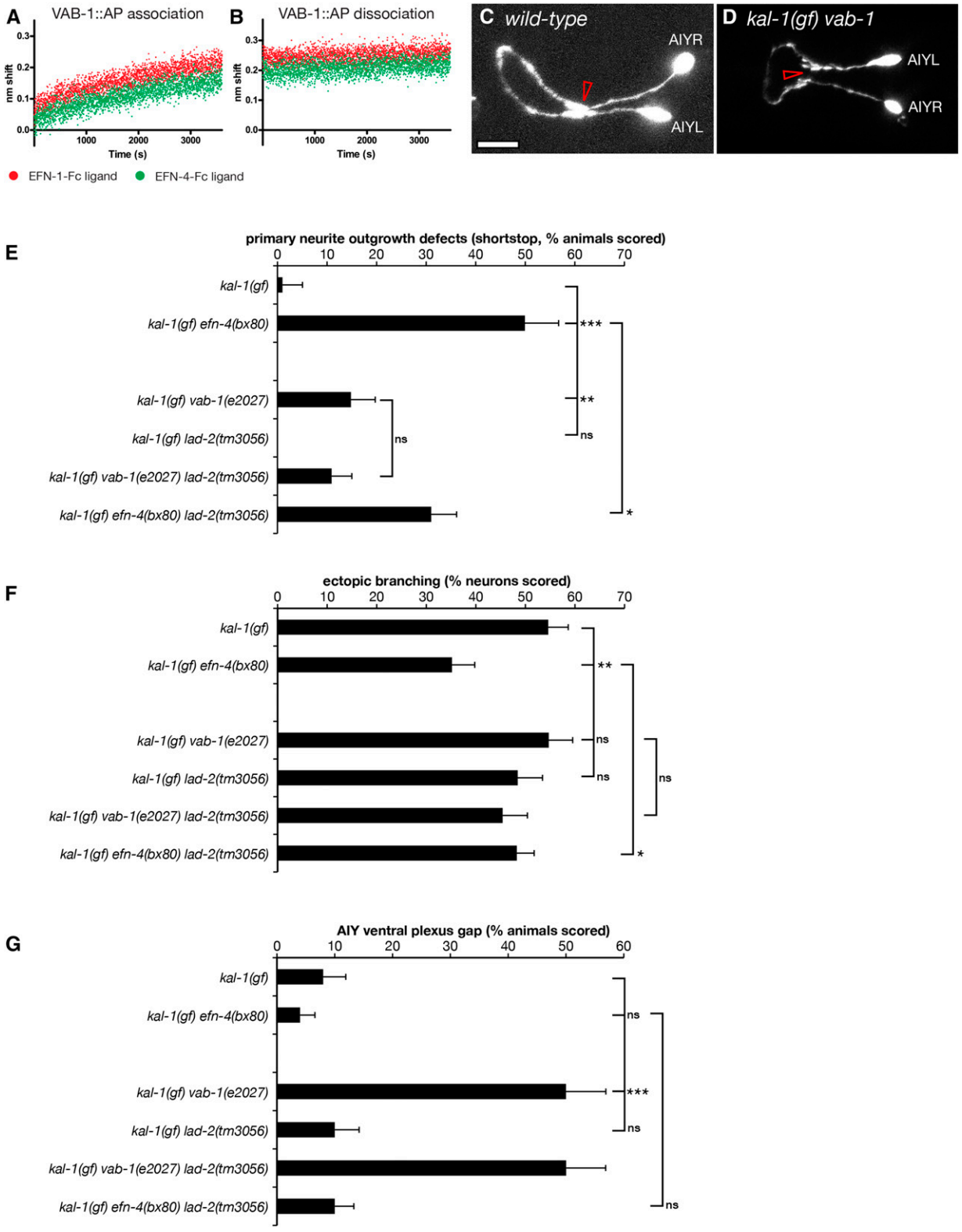

Figure 5 The Eph receptor *vab-1* promotes primary neurite outgrowth and ventral plexus contact in AIY neurons. Biolayer interferometry was used to demonstrate binding between the extracellular domain of VAB-1 fused to alkaline phosphatase and ephrins EFN-1 and EFN-4. (A) VAB-1::AP-binding association phase. (B) VAB-1::AP dissociation phase. Binding curves are normalized against an Fc control to correct for instrument drift. (C and D) Confocal micrographs of AIY neurons in (C) wild-type and (D) *kal-1(gf) vab-1(e2027)* mutants. Open arrowhead in C shows the ventral contact point in wild-type AIY pairs. (D) *vab-1* mutants show a highly penetrant ventral gap where the AIYL/R cells fail to contact each other. Mutations in the candidate EFN-4 receptors *vab-1*/EphR and *lad-2*/L1CAM were assayed for (E) primary neurite outgrowth, (F) ectopic axon branching, and (G) ventral plexus contact. Statistical significance was determined using the Z-test. $*P < 0.05$; $**P < 0.01$; $***P < 0.001$. Error bars are standard error of proportion.

EFN-4 may function in a parallel genetic pathway with SDN-1/syndecan in AIY primary neurite outgrowth

Heparan sulfate proteoglycans have multiple roles in nervous system development, and EphR/ephrin signaling has been shown to function in concert with HSPGs in mouse cortical neuron outgrowth (Van Vactor *et al.* 2006; Irie *et al.* 2008). In *C. elegans*, the single-pass trans-membrane HSPG SDN-1/syndecan is required for neuroblast migration, axon outgrowth, axon guidance, and post-embryonic cell migration in multiple *C. elegans* CNS cell types (Rhiner *et al.* 2005; Hudson *et al.* 2006; Díaz-Balzac *et al.* 2014; Kinnunen 2014). In addition, LON-2/glypican has roles in the left/right guidance choices of dorsal B-type (DB) motor neurons and other axon guidance events (Bülow *et al.* 2008; Gysi *et al.* 2013; Pedersen *et al.* 2013; Díaz-Balzac *et al.* 2014; Blanchette *et al.* 2015). GPN-1/glypican is redundantly required for embryonic neuroblast migration but has no other reported function in *C. elegans* development (Hudson *et al.* 2006). UNC-52/perlecan is required for muscle development during embryogenesis and also has roles in *kal-1(gf)*-dependent ectopic branching of AIY neurons (Rogalski *et al.* 1993; Díaz-Balzac *et al.* 2014). We found that single mutants of the HSPGs *sdn-1*/syndecan, *gpn-1*/glypican, and *lon-2*/glypican had no significant effect on AIY primary neurite outgrowth (Figure 6B). However, *sdn-1* loss-of-function mutations in combination with either *lon-2*/glypican or *gpn-1*/glypican showed low yet significant primary neurite outgrowth defects, revealing redundant roles in AIY outgrowth among the HSPGs.

The *kal-1(gf)* background strongly sensitized AIY neurons to loss of *sdn-1*/syndecan, in contrast to loss of *unc-52*, *gpn-1*, and *lon-2*, which individually had no effect on primary neurite outgrowth. *sdn-1* shortstop phenotypes were significantly enhanced to 18% for the *sdn-1(ok449)* weak loss-of-function allele and 44% for the *sdn-1(zh20)* null (Figure 6, A and C). *sdn-1(ok449)* is an in-frame deletion of the *sdn-1* locus that removes the two known HS attachment sites yet retains the trans-membrane and C terminus, including the conserved PDZ-binding domain (Minniti *et al.* 2004; Rhiner *et al.* 2005; Dejima *et al.* 2014; Kinnunen 2014). Northern blot analysis indicates that *sdn-1(ok449)* is expressed at the same levels as wild-type *sdn-1* (Minniti *et al.* 2004). This is in contrast to *sdn-1(zh20)*, which completely lacks *sdn-1* messenger RNA and behaves as a true null mutant (Rhiner *et al.* 2005). Intriguingly, SDN-1(ok449) appears to be phosphorylated at the C terminus, suggesting that it retains some function, despite the absence of HS-side chains (Minniti *et al.* 2004). The difference in phenotype penetrance observed in *sdn-1(ok449)* versus *sdn-1(zh20)* suggests that SDN-1 may have both HS-dependent and -independent roles in AIY primary neurite outgrowth.

We also found that *kal-1(gf)*; *sdn-1(zh20)* primary neurite outgrowth defects were partially but significantly suppressed by *gpn-1* mutations (Figure 6C). However, *kal-1(gf)*; *lon-2 sdn-1* and *kal-1(gf)*; *unc-52 sdn-1* double mutants were not significantly different from *kal-1(gf)*; *sdn-1* mutants alone. This further suggests that *lon-2* and *unc-52* have no obvious roles in AIY primary neurite outgrowth when assayed in a *kal-1(gf)* background.

AIY-specific expression of *gfp*::*sdn-1* suppressed the *sdn-1* primary neurite shortstop phenotype (Figure 7, $P < 0.05$, one of three lines tested, with a second line approaching significance), suggesting that SDN-1 functions cell autonomously. Conversely, expression of *gfp*::*gpn-1* from a *gpn-1* promoter was sufficient to increase primary neurite defects (one of three lines tested, $P < 0.01$). AIY-specific expression of *lon-2* showed a striking and significant increase in primary neurite shortstop defects (three of three lines tested, $P < 0.001$). Curiously, our *P-AIY-lon-2* transgenic lines showed highly penetrant loss of AIY cell bodies, which appeared to be transgene-specific (15% of *kenEx16* and 11% of *kenEx17* animals showed missing AIY cell bodies compared with 67% of *kenEx18* animals). In addition, we observed exuberant axon branching (multiple branches from a single neuron) and hyper-long axon branches (data not shown). Taken together, these data suggest that the shortstop phenotypes seen in *P-AIY-lon-2* animals may be influenced by the transgenic arrays titering out TTX-3, leading to neomorphic phenotypes similar to those seen in *ttx-3* weak loss-of-function mutations (Altun-Gultekin *et al.* 2001). Despite this, our data support cell-autonomous yet antagonistic roles for SDN-1/syndecan and GPN-1/glypican in AIY primary neurite outgrowth.

Specific HS modifications have been shown to play distinct roles in *C. elegans* nervous system development (Bülow and Hobert 2004; Rhiner *et al.* 2005; Gysi *et al.* 2013; Díaz-Balzac *et al.* 2014; Kinnunen 2014). We asked whether individual genes required for HS modification had any effect on AIY primary neurite outgrowth. Single mutants of *hse-5*/C5-epimerase, *hst-2*(2-*O*-sulfotransferase), *hst-6* (6-*O*-sulfotransferase), and *sul-1* (arylsulfatase) either had no effect on AIY primary neurites or were not significantly different when compared to wild-type controls (Figure 6D). This was also the case when these mutants were examined in the *kal-1(gf)* background (Figure 6E). Considering the phenotype seen in *sdn-1(ok449)* mutants, which is essentially an HS-minus version of the *sdn-1* gene, these data suggest that there is likely to be considerable redundancy between different HS sulfation patterns with regard to AIY primary neurite outgrowth.

The similarity in phenotypes between *efn-4* and *sdn-1* mutants suggests that they may function in a linear genetic pathway to govern AIY primary neurite growth. However, *efn-4*; *sdn-1* double mutants exhibit strong synthetic lethality, making it difficult to directly address this question in adult worms (Hudson *et al.* 2006). As *hst-6* mutants show the strongest primary neurite phenotype (Figure 6E, 8% outgrowth defects, 6/78 worms assayed), we asked whether *efn-4* had any genetic interaction with *hst-6* mutants. Sixty-four percent of *efn-4*; *hst-6* double mutants showed primary neurite shortstop defects (52/81 animals scored), which is additive but not significantly different from *efn-4* mutants alone (Figure

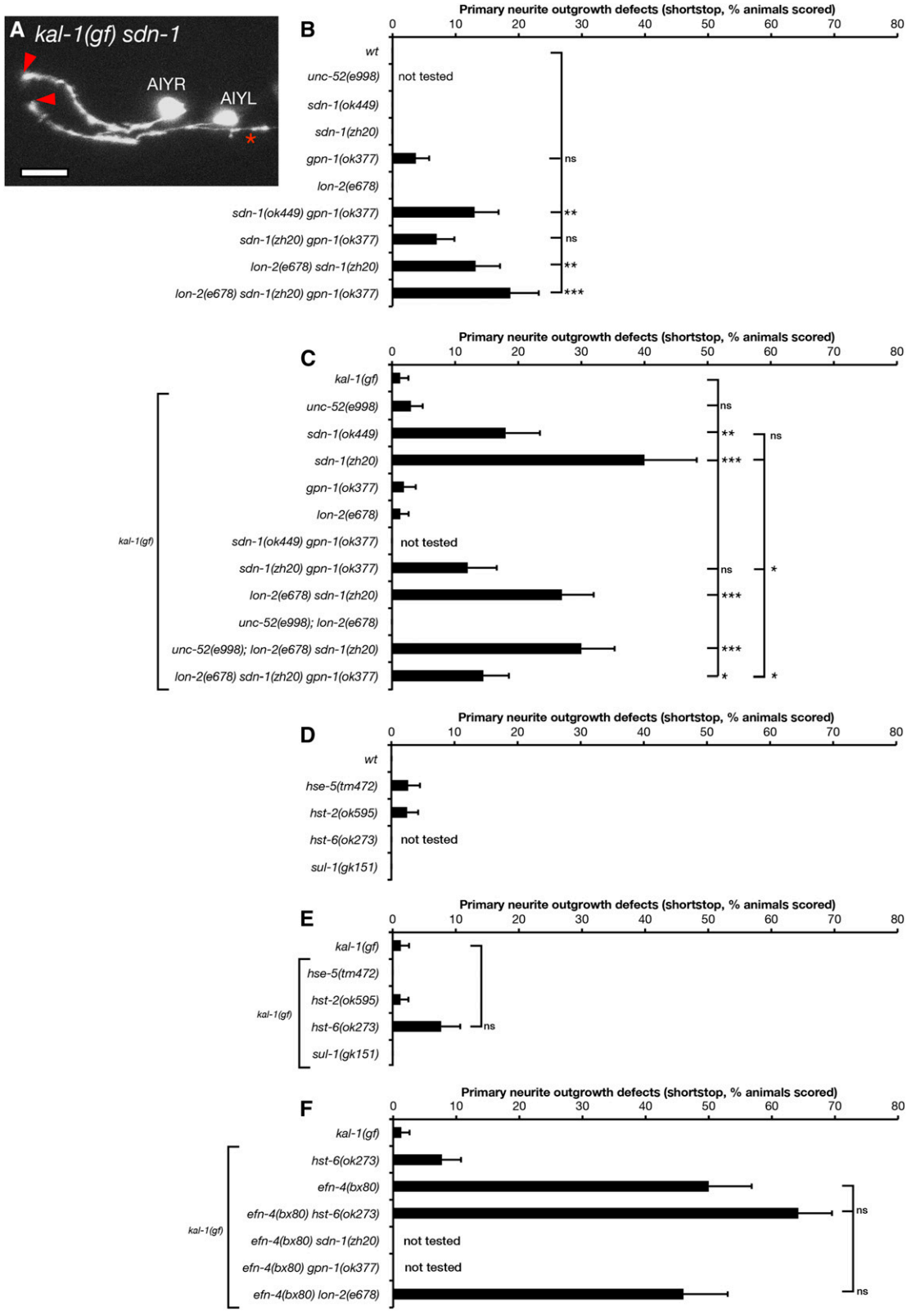

Figure 6 Heparan sulfate and heparan sulfate proteoglycans are required for AIY primary neurite outgrowth. (A) Confocal micrograph of AIY neuron morphology in a *kal-1(gf) sdn-1(zh20)* mutant. Arrowheads show premature termination of primary neurite outgrowth. Asterisk shows a *kal-1(gf)*-induced ectopic branch. Bar, 10 μm. (B–E) AIY primary neurite defects in HSPG core protein and HS-biosynthesis mutants assayed in *kal-1(gf)* and wild-type backgrounds. (F) AIY primary neurite defects in *efn-4(bx80)* double mutant combinations with either HSPG core protein or HS-biosynthesis mutants. Statistical significance was determined using the Z-test. $*P < 0.05$; $**P < 0.01$; $***P < 0.001$. Error bars are standard error of proportion.

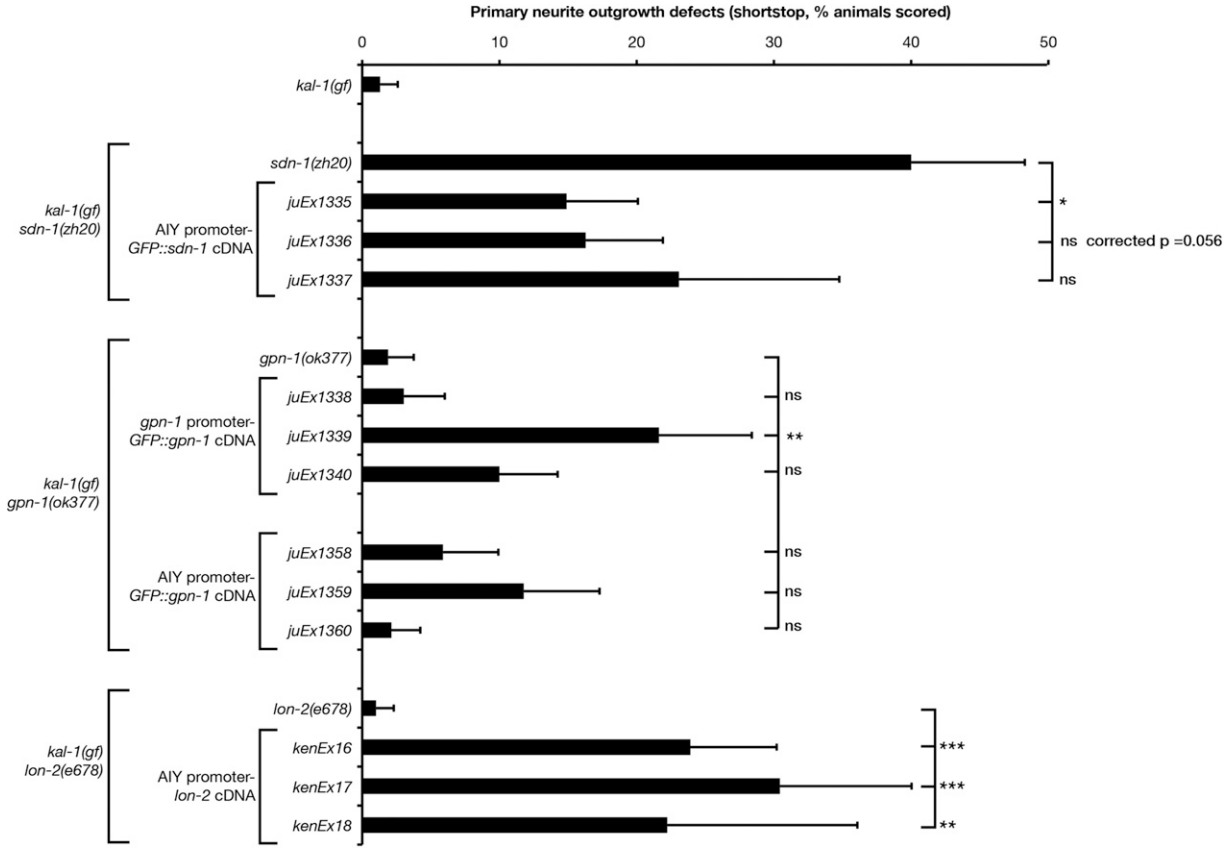

Figure 7 Cell-autonomous expression of heparan sulfate proteoglycans reveals opposing roles for SDN-1 and glypicans in AIY primary neurite outgrowth. Primary neurite defects in *kal-1(gf) HSPG* null mutants bearing transgenic rescue arrays. *sdn-1(zh20)* animals contain *P-AIY-sdn-1*::*GFP* transgenes. *gpn-1(ok377)* animals contain *P-gpn-1-gpn-1*::*GFP* or *P-AIY-gpn-1*::*GFP* transgenes. *lon-2(e678)* animals contain *P-AIY-lon-2* transgenes. *sdn-1*::*GFP* and *gpn-1*::*GFP* transgenes were previously shown to be functional (Hudson *et al.* 2006). *HSPG* null mutant data from Figure 6 are included for comparison. Statistical significance was determined using the Z-test. $*P < 0.05$; $**P < 0.01$; $***P < 0.001$. Error bars are standard error of proportion.

6F). Also, *efn-4*; *lon-2* double mutants show 46% axon outgrowth defects (23/50 animals scored), which is not significantly different from *efn-4* alone. From this, we conclude that both *sdn-1* and *efn-4* are required during AIY primary neurite extension although it is unclear if they function via a linear or parallel genetic pathway.

EFN-4 acts in parallel to the KAL-1/HSPG pathway in ectopic axon branching

KAL-1-dependent ectopic branching is strongly suppressed by mutations in the HS modification genes *hst-2*, *hst-3.2*, *hst-6*, and *hse-5*, indicating that this phenotype is an HS modification-dependent process (Bülow *et al.* 2002; Tecle *et al.* 2013). We confirmed some of these observations using deletion alleles of *hst-2*, *hst-6*, and *hse-5* (Figure 8B). We find that null mutations of HS modifier genes suppress *kal-1(gf)* branching to ~15–20% of AIY neurons, which is similar to that reported by others (Bülow *et al.* 2002).

The partial suppression of *kal-1(gf)* ectopic neurite branching and our data indicating that *efn-4* and *sdn-1* have similar roles during AIY primary neurite outgrowth suggests that *efn-4* may function in parallel with HSPGs during axon branching, similar to its role in embryogenesis (Hudson *et al.* 2006). Consistent with this interpretation, *efn-4*; *hst-6* double mutants caused significant suppression of *kal-1(gf)* branching to background levels (5%) compared to *hst-6* alone (15%, Figure 8B). We conclude that EFN-4 and HSPGs have parallel and partly redundant roles in KAL-1-induced ectopic neurite branching.

We also tested requirements for another HS modifier enzyme not previously examined for its roles in *kal-1(gf)* branching. *sul-1* encodes the *C. elegans* ortholog of the mammalian extracellular sulfatase Sulf1 (Ai *et al.* 2003; Nawroth *et al.* 2007). The deletion mutation *sul-1(gk151)* is predicted to eliminate most of the conserved functional domains of SUL-1 and thus cause either complete or strong loss of function. *sul-1(gk151)* animals were viable and fertile. We found that *sul-1* strongly suppressed *kal-1(gf)* branching (25%). As SUL-1 is predicted to remove 6-*O*-sulfate groups from sulfated *N*-acetylglucosamine residues of HSPGs, this result suggests that KAL-1 may be unable to interact with oversulfated HS.

We next examined the roles of HSPG core proteins in AIY neuron ectopic branch formation (Figure 8). Our previous analysis of embryonic morphogenesis identified the cell-surface HSPGs syndecan SDN-1 and glypican GPN-1 as acting

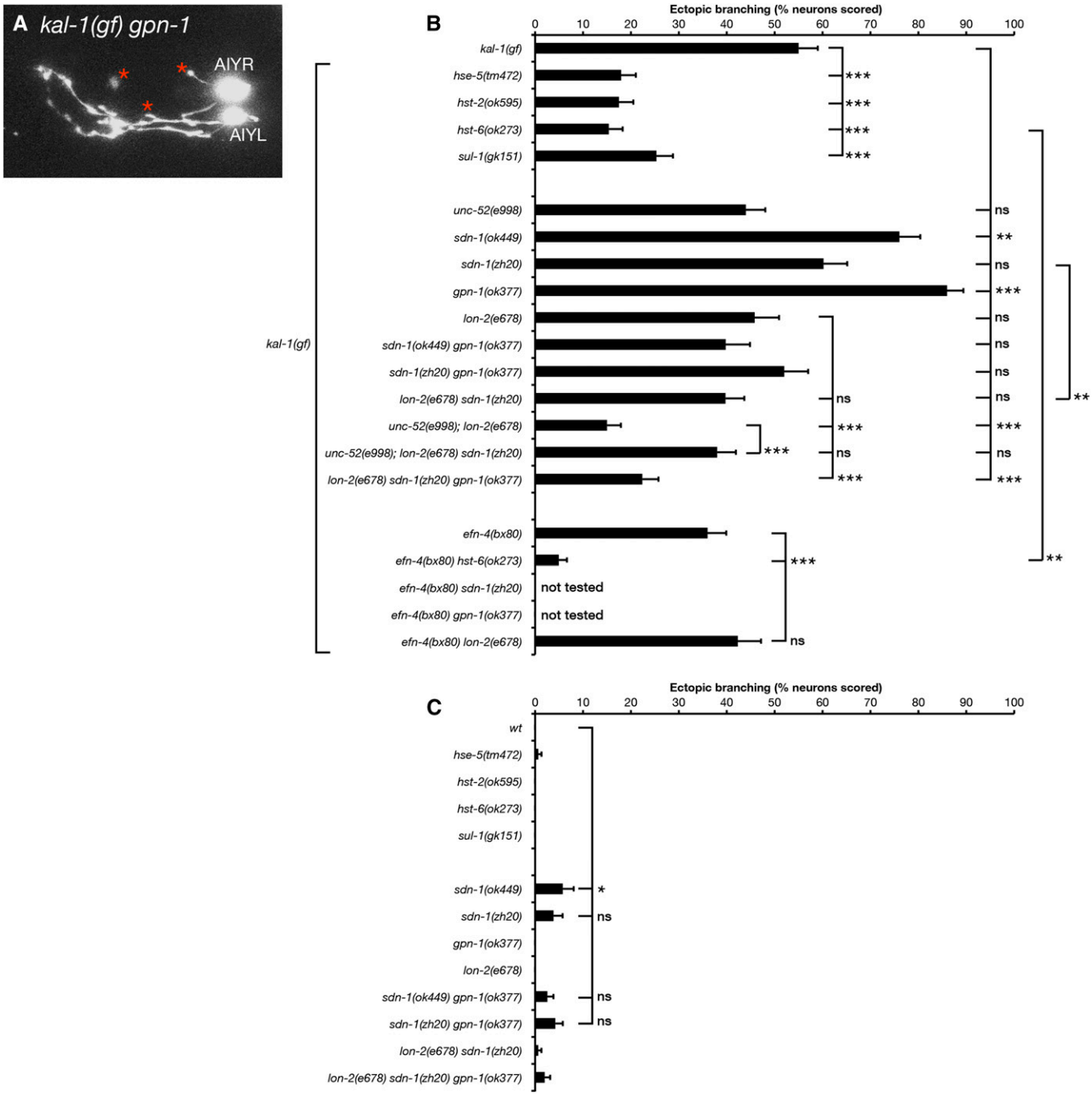

Figure 8 Heparan sulfate and heparan sulfate proteoglycans are required for *kal-1(gf)*-induced ectopic AIY neuron branching and function in parallel with EFN-4. (A) Confocal micrograph of AIY neurons in a *kal-1(gf) gpn-1(ok377)* mutant. Asterisks show exuberant branching. (B and C) AIY ectopic branching defects in HS biosynthesis and HSPG core protein mutants assayed in (B) *kal-1(gf)* and (C) wild-type backgrounds. Pertinent double-mutant combinations with *efn-4(bx80)* are also included. Statistical significance was determined using the Z-test. $*P < 0.05$; $**P < 0.01$; $***P < 0.001$. Error bars are standard error of proportion.

redundantly in a common pathway with KAL-1 (Hudson *et al.* 2006). In contrast to the requirement for SDN-1 in AIY neuron primary neurite outgrowth, we found that *sdn-1(ok449)* mutants showed increased ectopic branching, although this phenotype was not observed in *sdn-1(zh20)* null mutants. This was surprising because SDN-1 appears to be the most abundant HSPG in the *C. elegans* nervous system; *sdn-1(ok449)* mutants display dramatically reduced levels of neuronal anti-stub 3G10 immunoreactivity, an antibody that detects HS attachment sites on HSPG core proteins following heparatinase digestion (Minniti *et al.* 2004). Similarly, *gpn-1(ok377)* mutants also showed increased ectopic branching (Figure 8, A and B), suggesting that GPN-1 plays an antagonistic role in this phenotype. However, *lon-2(e678)* and

unc-52(e998) single mutants showed no obvious effect on ectopic branching. We then tested whether HSPGs might act redundantly in KAL-1-induced branching. *sdn-1 gpn-1* double mutants showed either no suppression (*zh20 ok377*, 52%) or only partial suppression (*ok449 ok377*, 40%, not significant) of *kal-1(gf)* branching. *lon-2 sdn-1* double mutants displayed moderate but not significant branching suppression (40%), whereas *unc-52*; *lon-2* double mutants showed striking suppression of *kal-1(gf)* ectopic branching (15%, $P < 0.001$), which is the same as that displayed by *hst-6* mutants. *lon-2 sdn-1 gpn-1* triple null mutants were viable and also showed strong suppression of *kal-1(gf)* branching (22%, $P < 0.001$). Curiously, we found that *unc-52*; *lon-2 sdn-1* triple mutants were weaker suppressors of branching than the *unc-52*; *lon-2* double-mutant strain (38%, $P < 0.001$). This observation supports the idea that SDN-1 may function as a negative regulator of *kal-1(gf)* ectopic branching. Overall, we conclude that all four *C. elegans* HSPGs examined have complex and partly redundant roles in KAL-1-induced ectopic neurite branching.

We used genomic and tissue-specific rescue experiments to clarify the roles of SDN-1, GPN-1, and LON-2 in *kal-1(gf)* ectopic branching (Figure 9). AIY-specific expression of a *gfp*::*sdn-1* cDNA strongly suppressed ectopic branching phenotypes, suggesting that SDN-1 functions cell autonomously (three of three lines, $P < 0.01$). Expression of a *gpn-1*::*GFP* cDNA from the *gpn-1* promoter also significantly suppressed the *gpn-1(ok377)* hyper-branching phenotype back to levels seen in *kal-1(gf)* animals alone (three of three lines). This result was mirrored by AIY-specific *gpn-1* transgenic arrays, suggesting that GPN-1 also functions cell autonomously. Finally, genomic expression of *lon-2* showed significant increases in ectopic branching (one of three lines tested), as did AIY-specific expression of *lon-2* (one of three lines, $P < 0.01$), although this AIY-specific data should be viewed with caution based on the neomorphic missing cell phenotype mentioned previously. Epidermal expression of *lon-2* had no effect on ectopic branching but did rescue *lon-2* mutant body-length defects (Gumienny *et al.* 2007). Taken together, these data point to cell-autonomous, negative regulatory roles for both SDN-1 and GPN-1 in *kal-1(gf)* ectopic branching, with UNC-52 and LON-2 functioning redundantly as positive regulators of this phenotype (Figure 10). The *kal-1(gf)* branching phenotype is driven by overexpression of KAL-1, which is a known HS-binding protein (Bülow *et al.* 2002; Hudson *et al.* 2006). We conclude that KAL-1-dependent axon branching is likely to be caused by an imbalance between KAL-1 and its negative regulators SDN-1 and GPN-1, leading to overactivation of the KAL-1 pathway and exuberant axon branch formation. LON-2 and UNC-52 appear to function downstream of KAL-1 in a redundant and non-cell-autonomously manner. This conclusion is based on the strong branching suppression seen in *unc-52*; *lon-2* double mutants, the ability of genomic LON-2 to increase ectopic branching, and the muscle-specific expression of UNC-52 (Rogalski *et al.* 1993). The strong suppression of branching seen in *sdn-1 lon-2 gpn-1* triple mutants appears paradoxical at first, but could be reconciled if SDN-1 functions both upstream and downstream of KAL-1 during ectopic branch formation. Perhaps the simplest conclusion is that all HSPGs function redundantly in the *kal-1(gf)* phenotype, such that it requires the removal of two or more major HSPGs to strongly suppress ectopic branching. Finally, the robust branching suppression found in HS modification mutants underlines the importance of distinct HS sulfation patterns in this process, suggesting that a particular HS sulfation motif is required for KAL-1 function.

Discussion

The data presented here identify a novel role for the *C. elegans* ephrin EFN-4 in shaping neuronal morphology. EphR–ephrin signaling functions primarily in a contact-dependent manner during nervous system development. For example, countergradients of EphRs and ephrins presented in the mammalian superior colliculus provide axon-targeting information for retinal ganglion cell growth cones navigating from the developing retina (Flanagan 2006). In this context, the target neuronal tissue presents positional cues to a navigating neural cell type. Also, EphRs and ephrins expressed in developing rhombomeres help drive their segregation into individual units during vertebrate hindbrain development (Mellitzer *et al.* 1999). Again, this EphR–ephrin interaction is solely within the nervous system. Our data indicate a novel role for EFN-4 where it acts non-cell autonomously from the epidermis to provide an axon outgrowth cue to AIY neurons.

EFN-4 as an axon-targeting cue

While the non-cell-autonomous role of EFN-4 in AIY axon outgrowth is novel, there is extensive evidence of non-cell-autonomous roles for other molecules in nervous system development. For example, UNC-6/netrin expression in the ventral epidermis provides pioneer growth cues to motorneurons during development of the nervous system (Wadsworth *et al.* 1996). In addition, SLT-1 expression from dorsal body-wall muscles guides AVM neuron axon path finding (Hao *et al.* 2001). While the netrin, slit/robo, and EphR/ephrin pathways have key roles in many aspects of nervous system development, both netrin and slit are secreted guidance cues, whereas ephrins are anchored to the cell membrane. In addition, AIY axon trajectories in *efn-4* mutants are normal in that both AIYL/R axons enter the nerve ring at the correct location, but stop short of their dorsal target. This suggests that EFN-4 is required, in part, to promote the final step of AIY primary neurite extension. Our previous work demonstrated a distinct region of EFN-4 expression in the anterior epidermis of lima bean stage embryos (Nakao *et al.* 2007). We speculate that this abrupt EFN-4 expression boundary may provide the guidance information required for AIY primary neurites to complete their dorsal migration.

Our rescue data hint that EFN-4 presented by the nascent pharynx may be partially required for AIY axon outgrowth (Figure 4). In support of this, EFN-4::GFP expression is

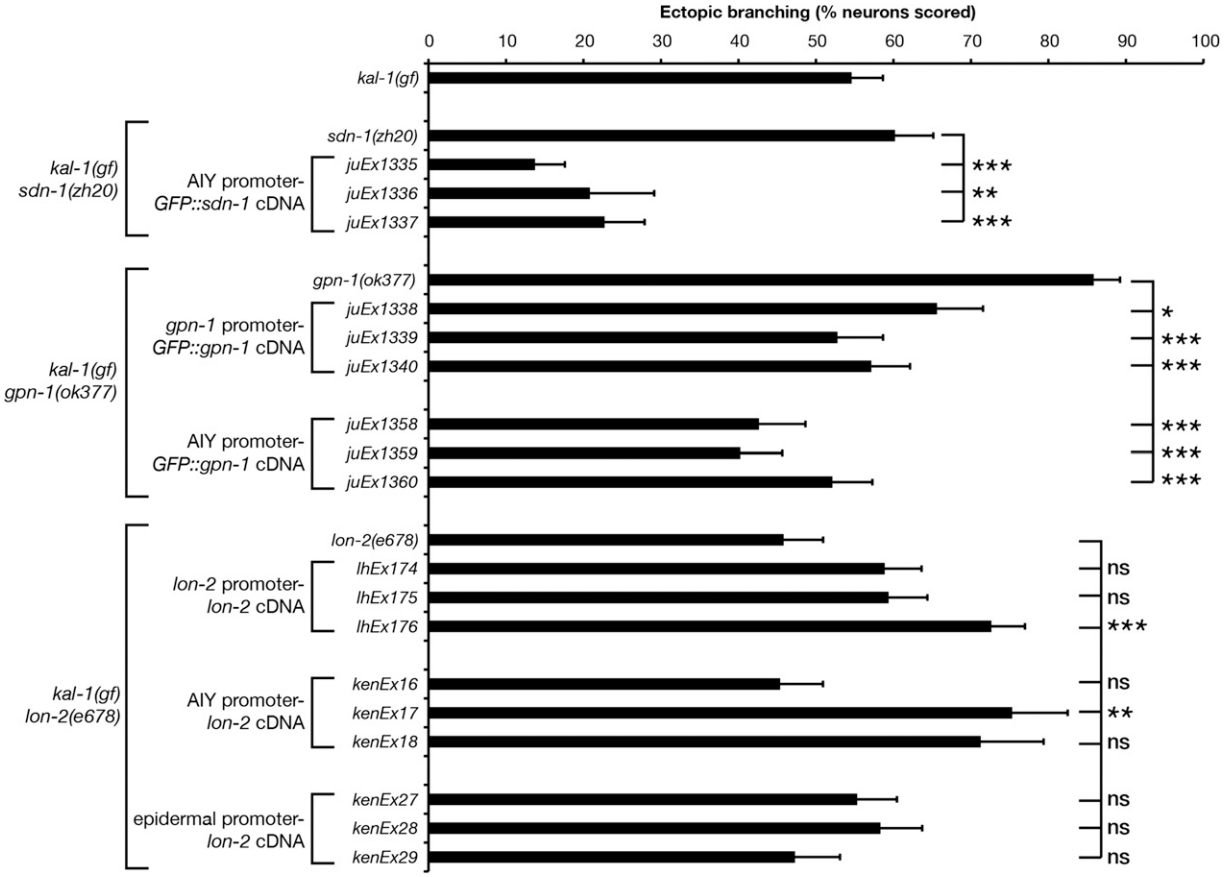

Figure 9 Overexpression of HSPG core proteins SDN-1 and GPN-1 can suppress *kal-1(gf)*-induced ectopic AIY neuron branching. Ectopic branching in *kal-1(gf) HSPG* null mutants bearing transgenic rescue arrays. *kal-1(gf)* ectopic branching defects in *sdn-1(zh20)* animals containing *P-AIY-sdn-1*::*GFP* transgenes; *gpn-1(ok377)* animals containing genomic-*gpn-1*::*GFP* and *P-AIY-gpn-1*::*GFP* transgenes; and *lon-2(e678)* animals containing genomic-*lon-2*, *P-AIY-lon-2*, and epidermis-specific-*lon-2* transgenes. *sdn-1(zh20)*, *gpn-1(ok377)*, and *lon-2(e678)* single-mutant data from Figure 8 are included for comparison. Statistical significance was determined using the Z-test. $*P < 0.05$; $**P < 0.01$; $***P < 0.001$. Error bars are standard error of proportion.

observed in pharyngeal tissue (Chin-Sang *et al.* 2002). Also, growth cones have already begun to migrate and encircle the developing pharynx at the lima bean stage, which is the earliest onset of *P-ttx-3-GFP* expression in AIY interneurons (Christensen *et al.* 2011 and our unpublished observations). While our most robust rescue data are driven from an *elt-3* epidermal promoter, it may be that EFN-4 presented from the pharynx can functionally compensate for epidermal EFN-4, bearing in mind that both tissues are close enough for cell–cell contact during this stage of AIY neuron development.

Canonical and noncanonical receptors for EFN-4

If EFN-4 is providing non-cell-autonomous growth cues to AIY axons, then there must be at least one receptor for EFN-4 being expressed on the AIY interneurons. The *C. elegans* genome contains only one predicted canonical EphR gene, *vab-1*. We find that *vab-1* mutations only partially phenocopy *efn-4* defects in axon outgrowth and instead exhibit a novel, highly penetrant ventral contact defect between the AIYL and AIYR cells. VAB-1 has a previously defined role in ventral midline axon fascicle maintenance, where it functions with EFN-1 and the cell-surface immunoglobulin superfamily protein WRK-1 (Boulin *et al.* 2006). In *C. elegans* embryos, EFN-1 and WRK-1 expression in the embryonic motor neuron cell bodies functions as a ventral midline pioneer cue for PVQ, HSN, and command interneurons. Expression of VAB-1 in the HSN neurons alone is sufficient to rescue *vab-1* HSN guidance defects. Also, VAB-1 can physically interact in a complex with WRK-1 and EFN-1. Whether WRK-1 or EFN-1 has roles in AIYL/R plexus contact remains to be determined.

Previous genetic data suggest that EFN-4 may represent a novel, noncanonical member of the *C. elegans* ephrin family; *vab-1* mutants have striking head and tail morphology defects, a phenotype shared with *efn-1* mutants, whereas *efn-4* mutants display only partially penetrant midbody and tail defects (George *et al.* 1998; Chin-Sang *et al.* 1999, 2002). In addition, *vab-1*; *efn-4* double null mutants exhibit synthetic embryonic lethality, suggesting that EFN-4 and VAB-1 each have one or more novel interaction partners during *C. elegans* embryogenesis. In addition to VAB-1's previously demonstrated binding interaction with WRK-1, it has also been shown to physically bind to SAX-3/robo (Ghenea *et al.* 2005; Boulin *et al.* 2006). Also, *sax-3* mutants share similar head morphology and axon outgrowth defects with *vab-1*

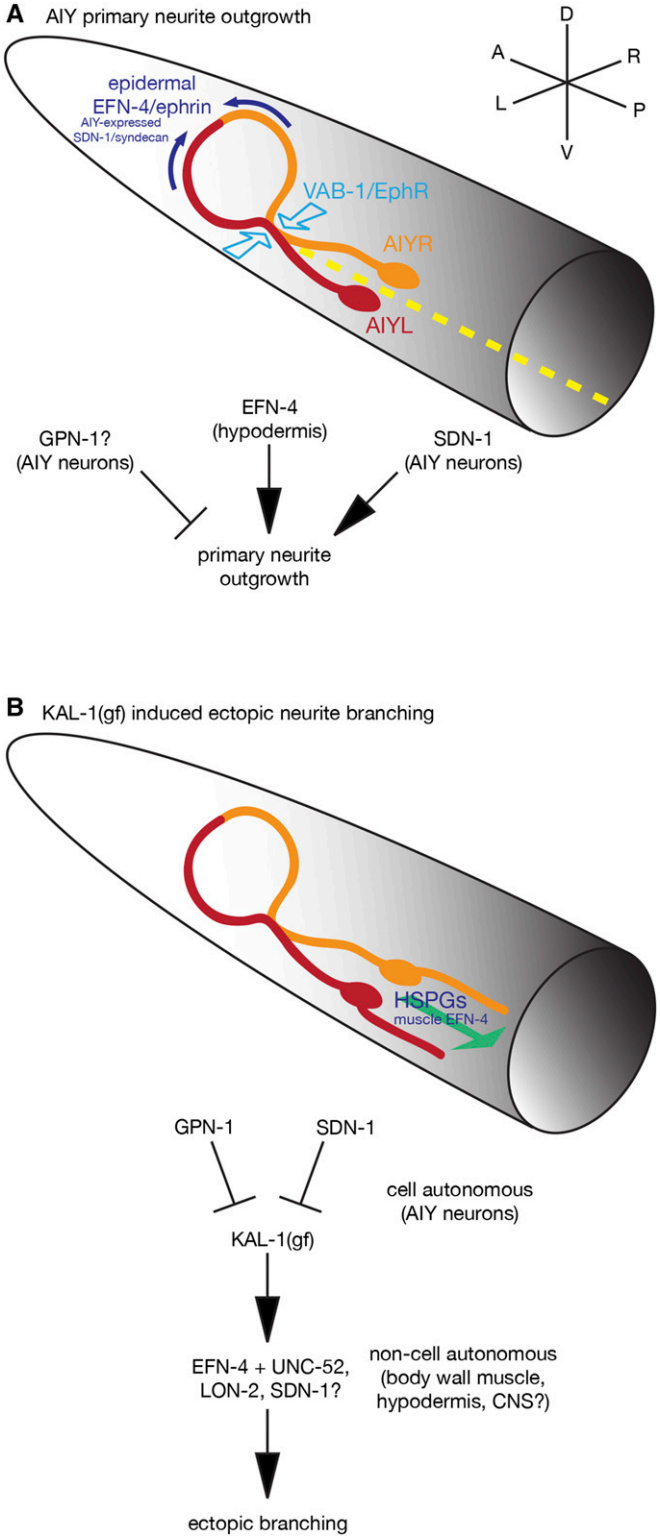

Figure 10 EFN-4 functions in concert with VAB-1 and HSPGs to shape AIY interneuron morphology in both wild-type and *kal-1(gf)* contexts. (A) Model summarizing the roles of EFN-4, SDN-1, and VAB-1 in promoting AIY interneuron primary neurite outgrowth. EFN-4, functioning non-autonomously from the epidermis, and SDN-1, functioning cell-autonomously in the AIY neurons, promote extension of the AIY primary neurites toward the dorsal midline but have no obvious roles in axon guidance. GPN-1 appears to function cell autonomously as a negative regulator of primary neurite outgrowth. VAB-1 has a minor role in nerve ring primary neurite extension but has a major role in driving AIYL/R contact in the ventral plexus. Whether VAB-1 is functioning cell autonomously in this process remains to be determined. The L1CAM LAD-2 may partially suppress EFN-4's role in primary neurite outgrowth (not shown). Dashed yellow line illustrates the ventral midline. (B) *kal-1 (gf)*-induced ectopic neurite branching is genetically distinct from primary neurite outgrowth. This phenotype is intrinsically cell autonomous, being driven from an integrated AIY-specific *kal-1* overexpression array. EFN-4 is required, in part, to promote secondary neurite branching where it functions non-cell autonomously in the body-wall muscle. Ectopic branches can be found emanating from either the cell bodies or the ventral portion of the primary neurite (for clarity, only a cell body branch has been shown). HS plays a major role in *kal-1(gf)*-induced ectopic branching, as loss of any of the HS-modifying enzymes HST-2, HST-6, HSE-5, or SUL-1 strongly suppresses this phenotype. The roles of HSPG core proteins in this phenotype are complex. Overexpression experiments indicate that GPN-1 and SDN-1 likely function as cell-autonomous regulators of *kal-1 (gf)* branching; SDN-1 promotes ectopic branching whereas GPN-1 inhibits branch outgrowth. *unc-52*; *lon-2* double-mutant and *sdn-1 gpn-1 lon-2* triple-mutant data, coupled with previously published expression data, suggest non-cell autonomous roles for LON-2 and UNC-52 in promoting axon branching and highlight the overlapping and partly redundant roles for HSPGs in this process. Whether loss of function on one HSPG core protein leads to longer HS branches on other core proteins is not known, but could provide a molecular explanation behind some of the core protein redundancy. Although our data indicate that no other HSPGs are involved, there may still be partly redundant roles for CLE-1/collagen XVIII or other cryptic HSPGs in this process.

mutants (Hao *et al.* 2001; Ghenea *et al.* 2005). Curiously, the highly penetrant body morphology defects found in *sax-3* mutants are at odds with those presented by *slt-1* mutants, which are essentially wild type in appearance. Taken together, these observations suggest caution when drawing conclusions based on genetic interactions alone.

Our optical biosensing data have helped to clarify the conundrum presented by *vab-1* and *efn-4*'s dissimilar mutant phenotypes. We find that the VAB-1 extracellular domain can bind rapidly to both EFN-1 and EFN-4 in vitro. This interaction is qualitatively high affinity in that we see no dissociation of VAB-1 from the EFN-1- and EFN-4-coated biosensors (Figure 5, A and B). Our data support previous findings, demonstrating that Fc-fusion proteins of EFN-1, -2, -3, and -4 can immunoprecipitate VAB-1 expressed in transiently transfected COS-1 cells (Wang *et al.* 1999). In addition, the intimate juxtaposition of EFN-4-expressing epidermal cells with VAB-1-expressing ventral neurons suggests that a physical interaction can occur between EFN-4 and VAB-1 during embryogenesis (George *et al.* 1998; Chin-Sang *et al.* 1999, 2002; Nakao *et al.* 2007). While our data suggest a role for VAB-1 in promoting EFN-4-dependent primary neurite extension, we also find that at least one other receptor is required for this process. Although L1CAM LAD-2 may have a modest role in inhibiting EFN-4-dependent primary neurite outgrowth, it is unlikely to be the EFN-4 receptor required for neurite extension, raising the possibility that one or more novel EFN-4 receptors exist.

EFN-4 has genetically distinct roles in kal-1 gain-of-function ectopic branching

In addition to defining a role for EFN-4 in AIY primary neurite outgrowth, we find that EFN-4 is also required, in part, for *kal-1(gf)*-dependent ectopic neurite branching (Bülow *et al.* 2002). While the correlation between primary versus secondary neurite growth might seem obvious at first, we find that these two processes are genetically distinct. Epidermal expression of EFN-4 does not rescue ectopic neurite outgrowth, whereas muscle expression of EFN-4 does. Cell tracking data and *myo-3-GFP* transgene studies reveal that myoblasts are born adjacent to the AIY interneurons, making it possible that muscle expression of EFN-4 is at least partially required for ectopic secondary neurite outgrowth (Bao *et al.* 2006; Tucker and Han 2008).

In addition, UNC-52/perlecan, which is exclusively expressed in body-wall muscle, has a previously defined role in *kal-1(gf)* ectopic neurite branching (Díaz-Balzac *et al.* 2014). How EFN-4, a GPI-anchored ephrin, has multiple developmental effects on a single neuron is not known. It may be that distinct receptors are required for primary neurite outgrowth versus *kal-1(gf)*-dependent ectopic branching. Alternatively, the timing of ectopic branch formation may be different from primary neurite outgrowth, allowing an alternate cofactor or receptor to be expressed or recruited. Finally, receptors for EFN-4 may be localized to distinct and nonoverlapping domains on the AIY neurons, allowing a single ephrin to promote both primary neurite outgrowth and ectopic branch formation simultaneously.

SDN-1 and glypicans have opposing roles in both primary neurite outgrowth and ectopic branching

Previous studies have demonstrated the importance of HSPGs in nervous system development, where they have roles in TGFβ, Hedgehog, Wnt, and Slit/robo signaling (Perrimon and Hacker 2004; Yan and Lin 2008; Schaefer and Schaefer 2010; Taneja-Bageshwar and Gumienny 2012). Despite this, little is known about how HSPGs and EphR/ephrin pathways function in concert. Studies in mouse reveal that both HSPGs and ephrin-A3 function together during mouse cortical axon outgrowth (Irie *et al.* 2008). Also, retinal ganglion cells require HSPGs and Slit for accurate navigation at the optic chiasm (Plump *et al.* 2002; Pratt *et al.* 2006). Hence retinal ganglion cells require both HS and EphR/ephrin cues at distinct phases of neural development. Our data suggest that both EFN-4 and HSPGs are required during AIY primary neurite outgrowth. The *kal-1(gf)* background employed in much of our work sensitizes the AIY neurons to *sdn-1* loss of function, revealing primary neurite outgrowth defects similar to those seen in *efn-4* mutations. Also, cell-autonomous expression of *sdn-1* in the AIY neurons strongly suppresses *sdn-1* primary neurite extension defects. This suggests that SDN-1/syndecan has a cell-autonomous role in promoting AIY primary neurite outgrowth, which is in broad agreement with previously published data on the role of SDN-1 in other neuron cell types (Minniti *et al.* 2004; Rhiner *et al.* 2005; Bülow *et al.* 2008; Kinnunen 2014).

Intriguingly, *sdn-1* phenotypes are suppressed by both *lon-2* and *gpn-1* mutations, whereas cell-autonomous expression of GPN-1 or LON-2 causes increased primary neurite outgrowth defects. *gfp*::*gpn-1* is expressed in both neural and non-neuronal cells (M. L. Hudson, unpublished observations) whereas LON-2 functions from the epidermis to negatively regulate TGFβ signaling (Gumienny *et al.* 2007). Our tissue-specific expression data strongly suggest a cell-autonomous role for GPN-1 glypican in negatively regulating KAL-1(gf) neurite extension. Also, the strong increase in *P-AIY-lon-2*-dependent primary neurite defects suggests that LON-2 may also be a negative regulator of outgrowth. However, we caution against a simple interpretation of this. First, there is no evidence of LON-2 expression in the nervous system (Gumienny *et al.* 2007). Second, we suspect that the *P-AIY-lon-2* lines may be exhibiting *ttx-3*-like weak loss-of-function phenotypes that are masking the underlying data (Altun-Gultekin *et al.* 2001). Despite these observations, our *lon-2* loss-of-function data are robust and continue to support a role for LON-2 during AIY primary neurite outgrowth and branching. This is consistent with previous work demonstrating partly redundant roles for LON-2 in nervous system development, including genetic and physical interactions between LON-2 and the axon guidance molecules UNC-40/DCC and UNC-6/netrin (Díaz-Balzac *et al.* 2014; Kinnunen 2014; Blanchette *et al.* 2015).

UNC-52 and LON-2 are redundantly required for ectopic branching

We also uncovered a cryptic role for UNC-52/perlecan during ectopic branch formation. Our data show that *unc-52*; *lon-2* double mutants strongly suppress ectopic branching, which is in good agreement with previously published data (Díaz-Balzac *et al.* 2014). This effect is likely to be non-cell autonomous; UNC-52 is exclusively expressed in the muscle whereas LON-2 is expressed only in the epidermis (Moerman *et al.* 1996). However, there is strong evidence that LON-2 can be shed from the cell surface and act at a distance (Taneja-Bageshwar and Gumienny 2012; Blanchette *et al.* 2015). In addition, UNC-52 is a secreted proteoglycan and associates with the basement membrane (Rogalski *et al.* 1993). It may be that both proteins contribute to the extracellular matrix, generating a HS-dependent permissive environment for ectopic neurite growth.

Heparan sulfate modifications have distinct roles in primary neurite outgrowth versus ectopic branch formation

During the course of this work, we also investigated the role of specific HS modifications in AIY primary neurite outgrowth and branching. We find that loss of individual HS modification enzymes leads to very weak phenotypes in primary neurite extension yet very strong phenotypes in ectopic neurite formation. *hst-6* shows the strongest primary neurite outgrowth

defect and is not significantly different from the HS-less *sdn-1(ok449)* allele, suggesting that 6-*O*-sulfated HS side chains may be required for this process. However, it is also possible that there is redundancy in HS sulfation and modification patterns such that different HS motifs can functionally compensate for one another during AIY primary neurite extension, similar to that reported for the genetic redundancy between *hst-2*, *hst-6*, and *hse-5* during dorsal A-type (DA) and DB motorneuron outgrowth (Bülow *et al.* 2008).

The ectopic branching phenotype seen in *kal-1(gf)* animals represents a Kallmann syndrome model and was originally used as a genetic screening background to identify novel genes that may be involved in this neurodevelopmental disorder (Bülow *et al.* 2002; Díaz-Balzac *et al.* 2014). We confirmed and extended these findings, revealing that multiple enzymes in the HS modification pathway are required for ectopic branch formation, including the arylsulfatase ortholog SUL-1. The role of HSPG core proteins in *kal-1(gf)* ectopic branching broadly parallels the roles of these proteins in primary neurite outgrowth, although there is considerable redundancy in their interplay. Our data strongly support cell-autonomous antagonistic roles between SDN-1 and GPN-1, functioning in *cis* in both primary neurite extension and ectopic branching. This is in contrast to the role of *dally/*glypican in *Drosophila*, which functions antagonistically and in *trans* with *Dsdn/*syndecan and LAR/receptor tyrosine phosphatase during neuromuscular junction development (Johnson *et al.* 2006).

All HS modification mutants examined in this work display striking suppression of *kal-1(gf)*-induced ectopic axon branching, illustrating the importance of epimerization and HS sulfation in this process and broadly agreeing with previously published data (Bülow *et al.* 2002; Tecle *et al.* 2013; Díaz-Balzac *et al.* 2014). However, these phenotypes are at odds when compared to those seen in individual HSPG core protein mutants alone, which show either no suppression or actually increased branching levels. Double- and triple-mutant combinations reveal significant genetic redundancy between these genes. The branching suppression seen in our *unc-52*; *lon-2* double mutant and *lon-2 sdn-1 gpn-1* triple mutant is not significantly different from that seen in our strongest HS-modifier suppressor mutant, *hst-6(ok273)*, confirming previous data on the importance of 6-*O*-sulfated HS to *kal-1(gf)* ectopic branching (Bülow *et al.* 2002). However, *unc-52*; *lon-2 sdn-1* triple mutants have significantly higher branching levels than *unc-52*; *lon-2* animals. This adds further evidence to the idea that *sdn-1* functions as an upstream negative regulator of KAL-1. An alternative explanation is that loss-of-function mutations in two key HSPGs increases the HS levels on core proteins that are not always HS-decorated, such as collagen XVIII (Ackley *et al.* 2005). A third possibility is that different splice variants of UNC-52 become HS-modified. Null mutations of *unc-52* are embryonic lethal (Rogalski *et al.* 1993; Moerman *et al.* 1996). The *unc-52(e998)* allele used in this study is viable, but raises the possibility that additional *unc-52* splice variants become HS-modified or increase their levels of HS decoration in the absence of *sdn-1*. Overall, our data indicate that UNC-52, SDN-1, GPN-1, and LON-2 function together to govern *kal-1(gf)* ectopic branching and that this process is intrinsically HS-dependent. It is also possible that additional HSPG core proteins play cryptic roles in this process.

EFN-4 and HSPGs function in parallel pathways to promote kal-1(gf) ectopic branching

Our previous analysis of KAL-1, SDN-1/syndecan, and GPN-1/glypican in embryogenesis indicated that all three genes function in parallel with EFN-4 (Hudson *et al.* 2006). In this study, we took advantage of the *kal-1(gf)* ectopic branching phenotype to further explore the genetic relationship between these genes. Unfortunately, the strong synthetic lethality seen between *sdn-1* and *efn-4* mutants makes it difficult to directly address their interplay during AIY neuron primary neurite outgrowth and ectopic branching. However, we have indirect evidence that they function in parallel pathways. In ectopic neurite branching, EFN-4 is clearly functioning in parallel with a pathway requiring 6-*O*-sulfated HS, as *efn-4*; *hst-6* double mutants show the strongest axon-branching suppression. Second, *lon-2* shows no genetic interaction with *efn-4*, beyond a modest increase in embryonic lethality (M.L. Hudson, unpublished observations), whereas *lon-2* can suppress *sdn-1* phenotypes. Taken together, we conclude that EFN-4 and HSPGs function in parallel to promote *kal-1(gf)* ectopic neurite branching (and probably AIY primary neurite outgrowth also), although other interpretations of these data are possible.

A possible role for multiple ephrins in shaping a single neuron?

Overall, our data point to a model where EFN-4 functions in the epidermis to promote AIY primary neurite outgrowth, possibly by binding to VAB-1 and one or more additional coreceptors (Figure 10). This interaction is in parallel with HSPGs, which function cell autonomously in primary neurite outgrowth. In addition, VAB-1 has a non-EFN-4-dependent role in shaping the ventral contact point between the AIYL and AIYR cells. Whether this is a cell-autonomous or non-cell-autonomous role for VAB-1 remains to be discovered. Intriguingly, an EFN-1::GFP reporter gene is expressed in the AIY interneurons, suggesting that VAB-1 may function non-cell autonomously to drive AIYL/R contact (Grossman *et al.* 2013). This raises the possibility that both VAB-1–EFN-1 and VAB-1–EFN-4 interactions are required to shape the overall morphology of AIY neurons. Careful dissection of the *C. elegans* EphR, ephrin, and HSPG promoter regions may define cell-specific enhancers that could be used for rescue assays to better understand the complex relationship between these highly conserved pathways.

Acknowledgments

We thank Kathryn Hudson, Philippe Mansour, Sebastian Chalfont, Lindsay Roe, and Mike Branden for help with

strain maintenance; Lihsia Chen for sharing reagents and data prior to publication; Hannes Bulow and Oliver Hobert for providing strains and alerting us to *efn-4*'s role in *kal-1 (gf)* axon branching; Susan Smith, Lihsia Chen, and anonymous reviewers for their thoughtful comments on the manuscript; and Erick Lee Purkhiser, R. Horton Heat, and Rusty Hodge for their inspiration during this work. Finally, we thank Wormbase, which is supported by National Institutes of Health (NIH) grant U41 HG002223, for additional resources. Some strains were provided by the *Caenorhabditis* Genetics Center, which is funded by the NIH Office of Research Infrastructure Programs (P40 OD010440). Additional strains were provided by Shohei Mitani and the National Bioresource Project, Tokyo Women's Medical University School of Medicine, Japan. M.L.H. was supported by a NIH Kansas IDeA Network of Biomedical Research Excellence fellowship, a Knights Templar Eye Foundation Inc. Pediatric Ophthalmology Research Grant, and awards from Kennesaw State University's Center for Excellence in Teaching and Learning and the Office of the Vice President for Research. This work was supported by NIH awards to J.L.M. (R15 GM080701), B.D.A. (P20 GM103638), and A.D.C. (R01 GM054657).

Literature Cited

Abdiche, Y., D. Malashock, A. Pinkerton, and J. Pons, 2008 Determining kinetics and affinities of protein interactions using a parallel real-time label-free biosensor, the Octet. Anal. Biochem. 377: 209–217.

Ackley, B. D., 2014 Wnt-signaling and planar cell polarity genes regulate axon guidance along the anteroposterior axis in C. elegans. Dev. Neurobiol. 74: 781–796.

Ackley, B. D., R. J. Harrington, M. L. Hudson, L. Williams, C. J. Kenyon *et al.*, 2005 The two isoforms of the Caenorhabditis elegans leukocyte-common antigen related receptor tyrosine phosphatase PTP-3 function independently in axon guidance and synapse formation. J. Neurosci. 25: 7517–7528.

Ai, X., A.-T. Do, O. Lozynska, M. Kusche-Gullberg, U. Lindahl *et al.*, 2003 QSulf1 remodels the 6-O sulfation states of cell surface heparan sulfate proteoglycans to promote Wnt signaling. J. Cell Biol. 162: 341–351.

Altun, Z. F., L. A. Herndon, C. A. Wolkow, C. Crocker, R. Lints *et al.*, (eds.) WormAtlas 2002-2015. http://www.wormatlas.org.

Altun-Gultekin, Z., Y. Andachi, E. L. Tsalik, D. Pilgrim, Y. Kohara *et al.*, 2001 A regulatory cascade of three homeobox genes, ceh-10, ttx-3 and ceh-23, controls cell fate specification of a defined interneuron class in C. elegans. Development 128: 1951–1969.

Bao, Z., J. I. Murray, T. Boyle, S. L. Ooi, M. J. Sandel *et al.*, 2006 Automated cell lineage tracing in Caenorhabditis elegans. Proc. Natl. Acad. Sci. USA 103: 2707–2712.

Bargmann, C. I., 1998 Neurobiology of the Caenorhabditis elegans genome. Science 282: 2028–2033.

Blanchette, C. R., P. N. Perrat, A. Thackeray, and C. Y. Benard, 2015 Glypican is a modulator of netrin-mediated axon guidance. PLoS Biol. 13: e1002183.

Boulin, T., R. Pocock, and O. Hobert, 2006 A novel Eph receptor-interacting IgSF protein provides C. elegans motoneurons with midline guidepost function. Curr. Biol. 16: 1871–1883.

Brenner, S., 1974 The genetics of *Caenorhabditis elegans*. Genetics 77: 71–94.

Bülow, H. E., and O. Hobert, 2004 Differential sulfations and epimerization define heparan sulfate specificity in nervous system development. Neuron 41: 723–736.

Bülow, H. E., K. L. Berry, L. H. Topper, E. Peles, and O. Hobert, 2002 Heparan sulfate proteoglycan-dependent induction of axon branching and axon misrouting by the Kallmann syndrome gene kal-1. Proc. Natl. Acad. Sci. USA 99: 6346–6351.

Bülow, H. E., N. Tjoe, R. A. Townley, D. Didiano, T. H. van Kuppevelt *et al.*, 2008 Extracellular sugar modifications provide instructive and cell-specific information for axon-guidance choices. Curr. Biol. 18: 1978–1985.

Cayuso, J., Q. Xu, and D. G. Wilkinson, 2015 Mechanisms of boundary formation by Eph receptor and ephrin signaling. Dev. Biol. 401: 122–131.

Chilton, J. K., 2006 Molecular mechanisms of axon guidance. Dev. Biol. 292: 13–24.

Chin-Sang, I. D., S. E. George, M. Ding, S. L. Moseley, A. S. Lynch *et al.*, 1999 The ephrin VAB-2/EFN-1 functions in neuronal signaling to regulate epidermal morphogenesis in C. elegans. Cell 99: 781–790.

Chin-Sang, I. D., S. L. Moseley, M. Ding, R. J. Harrington, S. E. George *et al.*, 2002 The divergent C. elegans ephrin EFN-4 functions inembryonic morphogenesis in a pathway independent of the VAB-1 Eph receptor. Development 129: 5499–5510.

Chisholm, A. D., and Y. Jin, 2005 Neuronal differentiation in C. elegans. Curr. Opin. Cell Biol. 17: 682–689.

Christensen, R., L. De La Torre-Ubieta, A. Bonni, and D. A. Colon-Ramos, 2011 A conserved PTEN/FOXO pathway regulates neuronal morphology during C. elegans development. Development 138: 5257–5267.

Dejima, K., S. Kang, S. Mitani, P. Cosman, and A. D. Chisholm, 2014 Syndecan defines precise spindle orientation by modulating Wnt signaling in C. elegans. Development 141: 4354–4365.

Díaz-Balzac, C. A., M. I. Lázaro-Peña, E. Tecle, N. Gomez, and H. E. Bülow, 2014 Complex cooperative functions of heparan sulfate proteoglycans shape nervous system development in *Caenorhabditis elegans*. G3 (Bethesda) 4: 1859–1870.

Díaz-Balzac, C. A., M. I. Lázaro-Peña, G. A. Ramos-Ortiz, and H. E. Bülow, 2015 The adhesion molecule KAL-1/anosmin-1 regulates neurite branching through a SAX-7/L1CAM-EGL-15/FGFR receptor complex. Cell Reports 11: 1377–1384.

Dodé, C., and J.-P. Hardelin, 2009 Kallmann syndrome. Eur. J. Hum. Genet. 17: 139–146.

Fire, A., S. W. Harrison, and D. Dixon, 1990 A modular set of lacZ fusion vectors for studying gene expression in Caenorhabditis elegans. Gene 93: 189–198.

Flanagan, J. G., 2006 Neural map specification by gradients. Curr. Opin. Neurobiol. 16: 59–66.

Franco, B., S. Guioli, A. Pragliola, B. Incerti, B. Bardoni *et al.*, 1991 A gene deleted in Kallmann's syndrome shares homology with neural cell adhesion and axonal path-finding molecules. Nature 353: 529–536.

George, S. E., K. Simokat, J. Hardin, and A. D. Chisholm, 1998 The VAB-1 Eph receptor tyrosine kinase functions in neural and epithelial morphogenesis in C. elegans. Cell 92: 633–643.

Ghenea, S., J. R. Boudreau, N. P. Lague, and I. D. Chin-Sang, 2005 The VAB-1 Eph receptor tyrosine kinase and SAX-3/Robo neuronal receptors function together during C. elegans embryonic morphogenesis. Development 132: 3679–3690.

Grossman, E. N., C. A. Giurumescu, and A. D. Chisholm, 2013 Mechanisms of ephrin receptor protein kinase-independent signaling in amphid axon guidance in *Caenorhabditis elegans*. Genetics 195: 899–913.

Gumienny, T. L., L. T. MacNeil, H. Wang, M. De Bono, J. L. Wrana *et al.*, 2007 Glypican LON-2 is a conserved negative regulator

of BMP-like signaling in Caenorhabditis elegans. Curr. Biol. 17: 159–164.
Gysi, S., C. Rhiner, S. Flibotte, D. G. Moerman, and M. O. Hengartner, 2013 A network of HSPG core proteins and HS modifying enzymes regulates netrin-dependent guidance of D-type motor neurons in Caenorhabditis elegans. PLoS One 8: e74908.
Hao, J. C., T. W. Yu, K. Fujisawa, J. G. Culotti, K. Gengyo-Ando *et al.*, 2001 C. elegans slit acts in midline, dorsal-ventral, and anterior-posterior guidance via the SAX-3/Robo receptor. Neuron 32: 25–38.
Harrington, R. J., M. J. Gutch, M. O. Hengartner, N. K. Tonks, and A. D. Chisholm, 2002 The C. elegans LAR-like receptor tyrosine phosphatase PTP-3 and the VAB-1 Eph receptor tyrosine kinase have partly redundant functions in morphogenesis. Development 129: 2141–2153.
Hayashi, Y., T. Hirotsu, R. Iwata, E. Kage-Nakadai, H. Kunitomo *et al.*, 2009 A trophic role for Wnt-Ror kinase signaling during developmental pruning in Caenorhabditis elegans. Nat. Neurosci. 12: 981–987.
Hobert, O., I. Mori, Y. Yamashita, H. Honda, Y. Ohshima *et al.*, 1997 Regulation of interneuron function in the C. elegans thermoregulatory pathway by the ttx-3 LIM homeobox gene. Neuron 19: 345–357.
Holen, H. L., L. Zernichow, K. E. Fjelland, I. M. Evenroed, K. Prydz *et al.*, 2011 Ephrin-B3 binds to a sulfated cell-surface receptor. Biochem. J. 433: 215–223.
Hu, Y., F. Tanriverdi, G. S. MacColl, and P.-M. G. Bouloux, 2003 Kallmann's syndrome: molecular pathogenesis. Int. J. Biochem. Cell Biol. 35: 1157–1162.
Huang, X., P. Huang, M. K. Robinson, M. J. Stern, and Y. Jin, 2003 UNC-71, a disintegrin and metalloprotease (ADAM) protein, regulates motor axon guidance and sex myoblast migration in C. elegans. Development 130: 3147–3161.
Hudson, M. L., T. Kinnunen, H. N. Cinar, and A. D. Chisholm, 2006 C. elegans Kallmann syndrome protein KAL-1 interacts with syndecan and glypican to regulate neuronal cell migrations. Dev. Biol. 294: 352–365.
Ikegami, R., H. Zheng, S.-H. Ong, and J. Culotti, 2004 Integration of semaphorin-2A/MAB-20, ephrin-4, and UNC-129 TGF-beta signaling pathways regulates sorting of distinct sensory rays in C. elegans. Dev. Cell 6: 383–395.
Ikegami, R., K. Simokat, H. Zheng, L. Brown, G. Garriga *et al.*, 2012 Semaphorin and Eph receptor signaling guide a series of cell movements for ventral enclosure in C. elegans. Curr. Biol. 22: 1–11.
Irie, F., M. Okuno, K. Matsumoto, E. B. Pasquale, and Y. Yamaguchi, 2008 Heparan sulfate regulates ephrin-A3/EphA receptor signaling. Proc. Natl. Acad. Sci. USA 105: 12307–12312.
Johnson, K. G., A. Tenney, A. Ghose, A. M. Duckworth, M. E. Higashi *et al.*, 2006 The HSPGs Syndecan and Dallylike bind the receptor phosphatase LAR and exert distinct effects on synaptic development. Neuron 49: 517–531.
Kallmann, F. J., W. A. Schoenfeld, and S. E. Barrera, 1944 The genetic aspects of primary eunuchoidism. Am. J. Ment. Defic. 48: 203–236.
Kennerdell, J. R., R. D. Fetter, and C. I. Bargmann, 2009 Wnt-Ror signaling to SIA and SIB neurons directs anterior axon guidance and nerve ring placement in C. elegans. Development 136: 3801–3810.
Killeen, M. T., and S. S. Sybingco, 2008 Netrin, Slit and Wnt receptors allow axons to choose the axis of migration. Dev. Biol. 323: 143–151.
Kim, C., and W. C. Forrester, 2003 Functional analysis of the domains of the C elegans Ror receptor tyrosine kinase CAM-1. Dev. Biol. 264: 376–390.
Kinnunen, T. K., 2014 Combinatorial roles of heparan sulfate proteoglycans and heparan sulfates in Caenorhabditis elegans neural development. PLoS One 9: e102919.
Klein, R., 2012 Eph/ephrin signalling during development. Development 139: 4105–4109.
Legouis, R., J. P. Hardelin, J. Levilliers, J. M. Claverie, S. Compain *et al.*, 1991 The candidate gene for the X-linked Kallmann syndrome encodes a protein related to adhesion molecules. Cell 67: 423–435.
Lisabeth, E. M., G. Falivelli, and E. B. Pasquale, 2013 Eph receptor signaling and ephrins. Cold Spring Harb. Perspect. Biol. 5: pii: a009159.
Mellitzer, G., Q. Xu, and D. G. Wilkinson, 1999 Eph receptors and ephrins restrict cell intermingling and communication. Nature 400: 77–81.
Miller, M. A., P. J. Ruest, M. Kosinski, S. K. Hanks, and D. Greenstein, 2003 An Eph receptor sperm-sensing control mechanism for oocyte meiotic maturation in Caenorhabditis elegans. Genes Dev. 17: 187–200.
Minniti, A. N., M. Labarca, C. Hurtado, and E. Brandan, 2004 Caenorhabditis elegans syndecan (SDN-1) is required for normal egg laying and associates with the nervous system and the vulva. J. Cell Sci. 117: 5179–5190.
Moerman, D. G., H. Hutter, G. P. Mullen, and R. Schnabel, 1996 Cell autonomous expression of perlecan and plasticity of cell shape in embryonic muscle of Caenorhabditis elegans. Dev. Biol. 173: 228–242.
Mohamed, A. M., and I. D. Chin-Sang, 2006 Characterization of loss-of-function and gain-of-function Eph receptor tyrosine kinase signaling in C. elegans axon targeting and cell migration. Dev Biol 290: 164–176.
Murray, J. I., Z. Bao, T. J. Boyle, M. E. Boeck, B. L. Mericle *et al.*, 2008 Automated analysis of embryonic gene expression with cellular resolution in C. elegans. Nat. Methods 5: 703–709.
Nakao, F., M. L. Hudson, M. Suzuki, Z. Peckler, R. Kurokawa *et al.*, 2007 The PLEXIN PLX-2 and the ephrin EFN-4 have distinct roles in MAB-20/Semaphorin 2A signaling in *Caenorhabditis elegans* morphogenesis. Genetics 176: 1591–1607.
Nawroth, R., A. Van Zante, S. Cervantes, M. McManus, M. Hebrok *et al.*, 2007 Extracellular sulfatases, elements of the Wnt signaling pathway, positively regulate growth and tumorigenicity of human pancreatic cancer cells. PLoS One 2: e392.
Pedersen, M. E., G. Snieckute, K. Kagias, C. Nehammer, H. A. B. Multhaupt *et al.*, 2013 An epidermal microRNA regulates neuronal migration through control of the cellular glycosylation state. Science 341: 1404–1408.
Perrimon, N., and U. Hacker, 2004 Wingless, hedgehog and heparan sulfate proteoglycans. Development 131: 2509–2511.
Plump, A. S., L. Erskine, C. Sabatier, K. Brose, C. J. Epstein *et al.*, 2002 Slit1 and Slit2 cooperate to prevent premature midline crossing of retinal axons in the mouse visual system. Neuron 33: 219–232.
Pratt, T., C. D. Conway, N. M. M.-L. Tian, D. J. Price, and J. O. Mason, 2006 Heparan sulphation patterns generated by specific heparan sulfotransferase enzymes direct distinct aspects of retinal axon guidance at the optic chiasm. J. Neurosci. 26: 6911–6923.
Rasband, W. S., 1997–2014 ImageJ, National Institutes of Health, Bethesda, MD (http://imagej.nih.gov/ij/).
Rhiner, C., S. Gysi, E. Fröhli, M. O. Hengartner, and A. Hajnal, 2005 Syndecan regulates cell migration and axon guidance in C. elegans. Development 132: 4621–4633.
Rogalski, T. M., B. D. Williams, G. P. Mullen, and D. G. Moerman, 1993 Products of the unc-52 gene in Caenorhabditis elegans are homologous to the core protein of the mammalian basement membrane heparan sulfate proteoglycan. Genes Dev. 7: 1471–1484.
Rugarli, E. I., E. Di Schiavi, M. A. Hilliard, S. Arbucci, C. Ghezzi *et al.*, 2002 The Kallmann syndrome gene homolog in C. elegans is involved in epidermal morphogenesis and neurite branching. Development 129: 1283–1294.

Sasakura, H., H. Inada, A. Kuhara, E. Fusaoka, D. Takemoto *et al.*, 2005 Maintenance of neuronal positions in organized ganglie by SAX-7, a Caenorhabditis elegans homolog of L1. EMBO J. 24: 1477–1488.

Schaefer, L., and R. Schaefer, 2010 Proteoglycans: from structural compounds to signaling molecules. Cell Tissue Res. 339: 237–246.

Taneja-Bageshwar, S., and T. L. Gumienny, 2012 Two functional domains in *C. elegans* glypican LON-2 can independently inhibit BMP-like signaling. Dev. Biol. 371: 66–76.

Tecle, E., C. A. Diaz-Balzac, and H. E. Bülow, 2013 Distinct 3-O-sulfated heparan sulfate modification patterns are required for kal-1-dependent neurite branching in a context-dependent manner in *Caenorhabditis elegans*. G3 (Bethesda) 3: 541–552.

Tornberg, J., G. P. Sykiotis, K. Keefe, L. Plummer, X. Hoang *et al.*, 2011 Heparan sulfate 6-O-sulfotransferase 1, a gene involved in extracellular sugar modifications, is mutated in patients with idiopathic hypogonadotrophic hypogonadism. Proc. Natl. Acad. Sci. USA 108: 11524–11529.

Tucker, M., and M. Han, 2008 Muscle cell migrations of C. elegans are mediated by the alpha-integrin INA-1, Eph receptor VAB-1, and a novel peptidase homologue MNP-1. Dev. Biol. 318: 215–223.

Van Vactor, D., D. P. Wall, and K. G. Johnson, 2006 Heparan sulfate proteoglycans and the emergence of neuronal connectivity. Curr. Opin. Neurobiol. 16: 40–51.

Wadsworth, W. G., H. Bhatt, and E. M. Hedgecock, 1996 Neuroglia and pioneer neurons express UNC-6 to provide global and local netrin cues for guiding migrations in C. elegans. Neuron 16: 35–46.

Wang, X., P. J. Roy, S. J. Holland, L. W. Zhang, J. G. Culotti *et al.*, 1999 Multiple ephrins control cell organization in C. elegans using kinase-dependent and -independent functions of the VAB-1 Eph receptor. Mol. Cell 4: 903–913.

Wang, X., W. Zhang, T. Cheever, V. Schwarz, K. Opperman *et al.*, 2008 The C. elegans L1CAM homologue LAD-2 functions as a coreceptor in MAB-20/Sema2 mediated axon guidance. J. Cell Biol. 180: 233–246.

White, J. G., E. Southgate, J. N. Thomson, and S. Brenner, 1986 The structure of the nervous system of the nematode Caenorhabditis elegans. Philos. Trans. R. Soc. Lond. B Biol. Sci. 12: 1–340.

Wilson, J. L., I. M. Scott, and J. L. McMurry, 2010 Optical biosensing: kinetics of protein A-IGG binding using biolayer interferometry. Biochem. Mol. Biol. Educ. 38: 400–407.

WormAtlas, Z. F. Altun, L. A. Herndon, C. Crocker, R. Lints *et al.* (eds.) 2002–2015. http://www.wormatlas.org

Yan, D., and X. Lin, 2008 Opposing roles for glypicans in Hedgehog signalling. Nat. Cell Biol. 10: 761–763.

Yochem, J., T. Gu, and M. Han, 1998 A new marker for mosaic analysis in *Caenorhabditis elegans* indicates a fusion between hyp6 and hyp7, two major components of the hypodermis. Genetics 149: 1323–1334.

Zhen, M., and Y. Jin, 1999 The liprin protein SYD-2 regulates the differentiation of presynaptic termini in C. elegans. Nature 401: 371–375.

Communicating editor: P. Sengupta

GENETICS

Supporting Information
www.genetics.org/lookup/suppl/doi:10.1534/genetics.115.185298/-/DC1

The *Caenorhabditis elegans* Ephrin EFN-4 Functions Non-cell Autonomously with Heparan Sulfate Proteoglycans to Promote Axon Outgrowth and Branching

Alicia A. Schwieterman, Alyse N. Steves, Vivian Yee, Cory J. Donelson, Melissa R. Bentley, Elise M. Santorella, Taylor V. Mehlenbacher, Aaron Pital, Austin M. Howard, Melissa R. Wilson, Danielle E. Ereddia, Kelsie S. Effrein, Jonathan L. McMurry, Brian D. Ackley, Andrew D. Chisholm, and Martin L. Hudson

DOI: 10.1534/genetics.115.185298

Table S1 ***efn-4*** **transgenic strain construction**

Strain numbers	Transgenic array	Plasmids
ATL20 – ATL22	*kenEx4 – 6*	pLC681 (5ng.ml^{-1})
	[P-myo-3::efn-4 + P-myo-3::mCherry]	pPD131-68 (25ng.ml^{-1})
		pBS II (20ng.ml^{-1})
ATL25 – ATL27	*kenEx9 – 11*	pMH853 (5ng.ml^{-1})
	[P-myo-2::efn-4 + P-myo-2::mCherry]	pBA183 (20ng.ml^{-1})
		pBS II (25ng.ml^{-1})
ATL28 – ATL30	*kenEx12 – 14*	pCZ148 (5ng.ml^{-1})
	[efn-4 genomic + P-ttx-3-RFP]*	pTTX-3-RFP (25ng.ml^{-1})
	** 5kb promoter*	pBS II (20ng.ml^{-1})
ATL35, ATL36	*kenEx19, 20*	pMH828 (5ng.ml^{-1})
	[P-unc-119-efn-4 + P-ttx-3::RFP]	pTTX-3-RFP (25ng.ml^{-1})
		pBS II (20ng.ml^{-1})
ATL50, ATL52	*kenEx21, 23*	pMH833 (5ng.ml^{-1})
	[P-elt-3-efn-4 + sur-5::GFP + P-ttx-3-RFP]	pTTX-3-RFP (10ng.ml^{-1})
		pTG96 (25ng.ml^{-1})
		pBS II (10ng.ml^{-1})
ATL63	*kenEx30*	pMH833 (0.5ng.ml^{-1})
	[P-elt-3-efn-4 + sur-5::GFP + P-ttx-3-RFP]	pTTX-3-RFP (10ng.ml^{-1})
		pTG96 (20ng.ml^{-1})
		pBS II (19.5ng.ml^{-1})
CZ6954 – CZ6956	*juEx1341 - 1343*	pMH340-3 (1ng.ml^{-1})
	[P-AIY-efn-4 + P-ttx-3-RFP]	pTTX-3-RFP (25ng.ml^{-1})
		pBS II (49ng.ml^{-1})

Table S2 HSPG transgenic strain construction

Strain	Transgenic array	Plasmids
CZ6948 – CZ6950	*juEx1335 - 1337*	pMH306-7 (1ng.ml^{-1})
	[P-ttx-3-GFP::sdn-1 cDNA + P-ttx-3-RFP]	pTTX-3-RFP (50ng.ml^{-1})
		pBS II (49ng.ml^{-1})
CZ6951 – CZ6953	*juEx1338 - 1340*	pMH265 (1ng.ml^{-1})
	[P-gpn-1-GFP::gpn-1 cDNA + P-ttx-3-RFP]	pTTX-3-RFP (50ng.ml^{-1})
		pBS II (49ng.ml^{-1})
CZ7064 – CZ7066	*juEx1358 - 1360*	pMH274 (5ng.ml^{-1})
	[P-ttx-3-gpn-1 cDNA + P-ttx-3-RFP]	pTTX-3-RFP (25ng.ml^{-1})
		pBS II (20ng.ml^{-1})
EVL491 – EVL493	*lhEx174 - 176*	pHW474 (5ng.ml^{-1})
	[P-lon-2-lon-2 cDNA + P-ttx-3-RFP]	pTTX-3-RFP (25ng.ml^{-1})
		pBS II (20ng.ml^{-1})
ATL60 – ATL62	*kenEx27 - 29*	pTG102 (5ng.ml^{-1})
	[P-elt-3-lon-2 cDNA + P-ttx-3-RFP]	pTTX-3-RFP (25ng.ml^{-1})
		pBS II (20ng.ml^{-1})
ATL32 – ATL34	*kenEx16 – 18*	pMH644 (5ng.ml^{-1})
	[P-ttx-3-lon-2 + P-ttx-3-RFP]	pTTX-3-RFP (25ng.ml^{-1})
		pBS II (20ng.ml^{-1})

Table S3. Temperature sensitivity of AIY primary neurite outgrowth defects ("short stop")

During the course of these studies, we observed that AIY primary neurite outgrowth was temperature sensitive. The table below illustrates the temperature sensitivity of *efn-4* axon outgrowth defects. The z-test was used to determine statistical significance between assay temperatures, i.e. *mgIs18 otIs76* assayed at 20°C was statistically compared to *mgIs18 otIs7*6 assayed at 25°C, etc. * $p < 0.05$, ** $p < 0.01$, *** $p < 0.001$.

Strain	% Short stop	Total animals scored
wt background		
mgIs18 efn-4(bx80) @15°C	23.1	78
mgIs18 efn-4(bx80) @20°C	33.8	77
mgIs18 efn-4(bx80) @25°C	32.0	75
mgIs18 efn-4(e1746ts) @15°C	17.9	78
mgIs18 efn-4(e1746ts) @ 20°C	21.3	75
mgIs18 efn-4(e1746ts) @ 25°C	38.5 (* cf. 20°C)	78
kal-1(gf) background		
mgIs18 otIs76 @15°C	0.0	76
mgIs18 otIs76 @20°C	1.3	77
mgIs18 otIs76 @25°C	9.1 (* cf. 20°C)	77
mgIs18 otIs76 efn-4(bx80) (@ 15°C)	35.1	77
mgIs18 otIs76 efn-4(bx80) (@ 20°C)	26.0	77
mgIs18 otIs76 efn-4(bx80) (@ 25°C)	40.5	79
mgIs18 otIs76 efn-4(e1746ts) @15°C	29.5	78
mgIs18 otIs76 efn-4(e1746ts) @ 20°C	19.8	81
mgIs18 otIs76 efn-4(e1746ts) @ 25°C	45.3 (*** cf. 20°C)	75
mgIs18 otIs76 efn-4(e36) (@15°C)	47.4	78
mgIs18 otIs76 efn-4(e36) (@20°C)	19.0 (*** cf. 15°C)	79
mgIs18 otIs76 efn-4(e36) (@25°C)	32.5	77

Table S4. Temperature sensitivity of *kal-1(gf)* AIY neuron ectopic axon branching

During the course of these studies, we also observed that the penetrance of *kal-1(gf)* ectopic axon branching was temperature sensitive. The table below shows three repeats of our axon branching assay run at 15, 20, and 25°C. The z-test was used to determine statistical significance between assay temperatures, i.e. *mgIs18 otIs76* assayed at 20°C was statistically compared to *mgIs18 otIs7*6 assayed at 25°C, etc. * $p < 0.05$, ** $p < 0.01$, *** $p < 0.001$.

Strain	% Branched AIYs	Significance		Total neurons scored
mgIs18 otIs76 @15°C – repeat 1	25.3			158
mgIs18 otIs76 @20°C – repeat 1	42.8	**		154
mgIs18 otIs76 @25°C – repeat 1	59.8		**	152
mgIs18 otIs76 @15°C – repeat 2	32.2			152
mgIs18 otIs76 @20°C – repeat 2	57.1	***		154
mgIs18 otIs76 @25°C – repeat 2	68.1		*	154
mgIs18 otIs76 (out-crossed 2x) @20°C – repeat 3	54.6			152
mgIs18 otIs76 (out-crossed 2x) @25°C – repeat 3	69.7	**		152
mgIs18 otIs76 efn-4(bx80) @ 15°C	30.5			154
mgIs18 otIs76 efn-4(bx80) @ 20°C	36.4	ns		154
mgIs18 otIs76 efn-4(bx80) @ 25°C	39.2		ns	158
mgIs18 otIs76 efn-4(e1746ts) @15°C	15.4			156
mgIs18 otIs76 efn-4(e1746ts) @ 20°C	35.8	***		162
mgIs18 otIs76 efn-4(e1746ts) @ 25°C	35.3		ns	150
mgIs18 otIs76 efn-4(e36) @15°C	21.2			156
mgIs18 otIs76 efn-4(e36) @20°C	36.1	**		158
mgIs18 otIs76 efn-4(e36) @25°C	38.7		ns	168

File S1 Construction of Fc-Mychis, EFN-1-Fc-Mychis and EFN-4-Fc-Mychis expression plasmids

pMH180 (Fc-Mychis expression vector) was built by PCR amplifying the Fc open reading frame from plasmid pCXFc-KAL (Bulow et al. 2002) using the primers below, digesting the PCR fragment with HindIII and EcoRI, then ligating into HindIII/EcoRI-digested pSecTagA (Life Technologies):

Forward primer: ATAAAGCTTCGACAAAACTCACACATG

Reverse primer: TATGAATTCTTTACCCGGAGACAGG

pMH873 (EFN-1ΔSecΔGPI-Fc-MycHis) was built by PCR amplifying the EFN-1 open reading frame from plasmid pLC708 (kind gift of Lihsia Chen) using the following primers:

Forward primer: AGGCGCGCCGTACGAAATCCCCTAGTGGAACGATATG

Reverse primer: GATCTTCccGAATTCTGCAAGcttCGACAAAACTCACACA

pMH874 (EFN-4ΔSecΔGPI-Fc-MycHis) was built by PCR amplifying the EFN-4 open reading frame from plasmid pMH828 (*P-unc-119-efn-4* cDNA) using the following primers:

Forward primer: AGGCGCGCCGTACGAAGcttAGACGAGCACATTGTCTAC

Reverse primer: AAAATCCTTGGAATATTtAAGcttCGACAAAACTCACACA

The *efn-1* and *efn-4* cDNAs PCR products were inserted into *Hind*III - linearized pMH180 using Gibson assembly (New England BioLabs), according to the manufacturer's protocol. All expression plasmids were sequenced then validated by transient transfection into 293T cells and Western blotting 48 hours later, using the anti-myc 9E10 antibody to detect the Myc tags.